

Quantum Computing for Query Containment of Conjunctive Queries

Luisa Gerlach
luisa.gerlach@hu-berlin.de
Humboldt-Universität zu Berlin
Berlin, Germany

Tobias Köppl
tobias.koeppel@fokus.fraunhofer.de
Fraunhofer-Institut für Offene
Kommunikationssysteme (FOKUS)
Berlin, Germany

René Zander
rene.zander@fokus.fraunhofer.de
Fraunhofer-Institut für Offene
Kommunikationssysteme (FOKUS)
Berlin, Germany

Nicole Schweikardt
schweikn@hu-berlin.de
Humboldt-Universität zu Berlin
Berlin, Germany

Stefanie Scherzinger
stefanie.scherzinger@uni-passau.de
Universität Passau
Passau, Germany

Abstract

We address the problem of checking query containment, a foundational problem in database research. Although extensively studied in theory research, optimization opportunities arising from query containment are not fully leveraged in commercial database systems, due to the high computational complexity and sometimes even undecidability of the underlying decision problem. In this article, we present the first approach to applying quantum computing to the query containment problem for conjunctive queries under set semantics. We propose a novel formulation as an optimization problem that can be solved on gate-based quantum hardware, and in some cases directly maps to quantum annealers. We formally prove this formulation to be correct and present a prototype implementation which we evaluate using simulator software as well as quantum devices. Our experiments successfully demonstrate that our approach is sound and scales within the current limitations of quantum hardware. In doing so, we show that quantum optimization can effectively address this problem. Thereby, we contribute a new computational perspective on the query containment problem.

The source code, data, and/or other artifacts have been made available at <https://github.com/miniHive/QC4QCoCQ>.

1 Introduction

The question of whether one query is contained in another is fundamental: it asks whether, for any possible input, the result of one query will always be a subset of the other. Being able to decide query containment opens numerous opportunities in data management, in particular query optimization, but also data integration, semantic caching, or access control. Variations of the problem have been studied in database theory for decades (cf. e.g. [7, 31, 33]), and for various query languages. Yet, due to the high computational cost of deciding query containment (NP-complete for conjunctive queries with set semantics) or outright infeasibility (undecidable for relational algebra), commercial database systems are restricted to using heuristics or rule-based rewrites. In this work, we focus on the query containment problem for conjunctive queries under set semantics (QC-CQ) [13]. In particular, we investigate whether this problem can be formulated for solving on quantum computers.

With access to commercially available quantum hardware, the database research community has begun to explore which core

database problems may benefit from offloading to quantum devices [11, 21, 47, 49, 50]. At this point, this line of research must remain very exploratory, as today’s early hardware prototypes are far from usable as co-processors in industrial-scale database systems. One limited resource is the number of available qubits or links (couplers) between them, often restricting experiments to solving toy examples. Further, today’s systems suffer from high levels of hardware noise that accumulates with increasing circuit size, so that results for larger inputs are often erroneous. Given the early technological state-of-the-art, the goal cannot yet realistically be to demonstrate a quantum advantage. Rather, we can ask how certain problems can be formulated so that they may eventually be offloaded to quantum hardware, once the technology reaches the required maturity and performance. At the same time, joining this quest early rather than late allows the database research community to take an active role in shaping quantum hardware and software ecosystems, as they emerge.

Much of recent research in this field focuses on formulating instances of optimization problems in QUBO form [22], where the objective is to minimize polynomials of degree at most two. This enables execution on quantum annealers, which currently provide access to thousands of qubits. Optimization problems involving higher-degree polynomials are typically addressed using the QAOA algorithm [18]. QAOA follows an annealing-inspired strategy but targets another hardware architecture: gate-based quantum processing units (QPUs), which can perform universal computations, yet are currently more restricted in the number of available qubits.

In the context of query optimization, the database research community has mainly been exploring the important task of join ordering [19, 29, 30, 36, 39, 44], as well as plan selection in multi-query optimization [17, 45]. These problems fall into the category of *cost-based query optimization*, where the aim is to choose among algebraically equivalent plans. In contrast, being able to decide query containment is a tool for *semantic query optimization*, and may allow to rewrite a given query into a simpler or smaller one. Yet to our knowledge, query containment has not yet been explored from a quantum computing perspective. Unlike many of the aforementioned query optimization tasks, there are no established classical implementations in today’s relational database systems with which to compete. This makes this problem particularly intriguing.

Contributions. This paper makes the following contributions.

1. We present a novel formulation of QC-CQ, the query containment problem for conjunctive queries under set semantics, as the problem of minimizing a polynomial. While related work oftentimes introduces such polynomials on the level of intuition, we formally prove our formulation to be correct.
2. Our problem formulation can be solved on quantum hardware. Specifically, polynomials with degree of up to 2 can be directly mapped to quantum annealers (which currently provide qubits in the range of thousands). For polynomials of arbitrary degree, we use QAOA on circuit-based QPUs (given enough qubits).
3. For future integration into a query engine, it is vital that our approach to containment checking only errs on the safe side. Otherwise, a query optimizer risks producing incorrect results. In fact, our approach is guaranteed to never produce any false positives, as all positives come with a verifiable witness.
4. We present a 3-stage workflow to decide QC-CQ. During pre-processing, we perform a simplification step, which we prove to be correct. Our experiments show that simplification is highly effective: by reducing the number of variables and the degree of the polynomial, the problem can be solved more efficiently.
5. Our experiments include simulators and real quantum hardware from leading vendors, using both quantum annealers and circuit-based QPUs. We evaluate soundness, scalability, and parameter sensitivity. In particular, we demonstrate the positive effects of using constraints in QAOA.
6. Our experiments indicate that there are instances of the containment problem that display energy landscapes that are particularly well-suited for our approach. This opens up a fresh perspective on the well-studied problem of query containment.

Structure. We review preliminaries on query containment and quantum computing (Sec. 2), before we derive our formalization for checking QC-CQ (Sec. 3). We present our workflow (Sec. 4) and its experimental evaluation (Sec. 5). We introduce a new perspective on containment problems by investigating their energy landscapes (Sec. 6), before we discuss our insights at a higher level of abstraction (Sec. 7). We review the related work (Sec. 8) and conclude (Sec. 9).

2 Preliminaries

2.1 Conjunctive Queries & Query Containment

We introduce conjunctive queries and the query containment problem, first by example and then formally. We assume set semantics, so relations and query results do not contain duplicate tuples. In formalizations, we adopt notation from Abiteboul, Hull, and Vianu [7].

Conjunctive Queries. We consider conjunctive queries that can be expressed by core SQL queries of the form “select distinct ... from ... where ...”, whose where-clause is a conjunction of equalities, and we use the syntax of *tableau queries* (cf., [7]) to express these queries. The following example is taken from [9, Chapter 15].

Example 2.1. Consider the schema consisting of three relations `Person[pid,pname,cid]`, `Profession[pid,pname]`, `City[cid,cname, country]` and the SQL query q_1 shown in Figure 1 on the left.

The same query can be expressed in the syntax of *tableau queries* (a language similar to *Query By Example (QBE)* [7]) via the *answer tuple* (Y_1) and the three relations shown on the right in Figure 1.

<pre>SELECT DISTINCT A.pname FROM Person A, Profession B, City C WHERE A.pid = B.pid AND B.pname = 'actor' AND A.cid = C.cid AND C.cname = 'L.A.' AND C.country = 'U.S.'</pre>	<table style="border-collapse: collapse; border: none;"> <tr> <td style="border-right: 1px solid black; padding: 2px 5px;">Person</td> <td style="padding: 2px 5px;">pid</td> <td style="padding: 2px 5px;">pname</td> <td style="padding: 2px 5px;">cid</td> </tr> <tr> <td style="border-right: 1px solid black; padding: 2px 5px;"></td> <td style="padding: 2px 5px;">X_1</td> <td style="padding: 2px 5px;">Y_1</td> <td style="padding: 2px 5px;">Z_1</td> </tr> <tr> <td style="border-right: 1px solid black; padding: 2px 5px;">Profession</td> <td style="padding: 2px 5px;">pid</td> <td style="padding: 2px 5px;">pname</td> <td></td> </tr> <tr> <td style="border-right: 1px solid black; padding: 2px 5px;"></td> <td style="padding: 2px 5px;">X_1</td> <td style="padding: 2px 5px;">'actor'</td> <td></td> </tr> <tr> <td style="border-right: 1px solid black; padding: 2px 5px;">City</td> <td style="padding: 2px 5px;">cid</td> <td style="padding: 2px 5px;">cname</td> <td style="padding: 2px 5px;">country</td> </tr> <tr> <td style="border-right: 1px solid black; padding: 2px 5px;"></td> <td style="padding: 2px 5px;">Z_1</td> <td style="padding: 2px 5px;">'L.A.'</td> <td style="padding: 2px 5px;">'U.S.'</td> </tr> </table>	Person	pid	pname	cid		X_1	Y_1	Z_1	Profession	pid	pname			X_1	'actor'		City	cid	cname	country		Z_1	'L.A.'	'U.S.'
Person	pid	pname	cid																						
	X_1	Y_1	Z_1																						
Profession	pid	pname																							
	X_1	'actor'																							
City	cid	cname	country																						
	Z_1	'L.A.'	'U.S.'																						

Figure 1: SQL query q_1 (left) and relations (right).

For answering this tableau query on a database instance, one strives for *valuations*, i.e., mappings v from the variables $\{X_1, Y_1, Z_1\}$ that occur in the query to the database entries, such that tuple $(v(X_1), v(Y_1), v(Z_1))$ belongs to relation `Person`, $(v(X_1), 'actor')$ belongs to relation `Profession`, and $(v(Z_1), 'L.A.', 'U.S.')$ belongs to relation `City`. Note how the tableau query uses shared variables, such as X_1 , to declare joins (as familiar from query languages like Datalog). The *query result* is the set of values $v(Y_1)$ for all such valuations v . Thus, the answer tuple is a means of declaring projections.

We now formalize these concepts. We write \mathbb{Z} for integers, \mathbb{N} for non-negative integers, and we let $\mathbb{N}_{\geq 1} := \mathbb{N} \setminus \{0\}$.

The *domain* of potential database entries is a fixed countably infinite set **dom**; elements in **dom** are called *constants*, and in concrete examples we will usually write them in quotes ‘...’. A *schema* is a finite set **S** of *relation names*, where each $R \in \mathbf{S}$ is equipped with a fixed *arity* $\text{ar}(R) \in \mathbb{N}$. A *database instance* of schema **S** (for short: **S**-db) is a mapping **I** that associates with each $R \in \mathbf{S}$ a finite relation $\mathbf{I}(R) \subseteq \mathbf{dom}^{\text{ar}(R)}$.

The conjunctive queries considered in this paper are defined as follows. We let **var** be an infinite set of *variables* with $\mathbf{var} \cap \mathbf{dom} = \emptyset$. A *free tuple* is an expression of the form (u_1, \dots, u_r) with $r \in \mathbb{N}$ and $u_1, \dots, u_r \in \mathbf{dom} \cup \mathbf{var}$. For a free tuple $u = (u_1, \dots, u_r)$ we let $\text{ar}(u) := r$ be the tuple’s *arity*, and we let $\text{vars}(u)$ and $\text{cons}(u)$ be the set of variables and constants, resp., that occur in u . For a set S of free tuples, we let $\text{vars}(S)$ and $\text{cons}(S)$ be the set of variables and constants, resp., that occur in some tuple in S .

A *conjunctive query* of schema **S** (for short: **S**-CQ) is of the form (\mathbf{T}, v) where **T** is a mapping that associates with each $R \in \mathbf{S}$ a finite set $\mathbf{T}(R)$ of free tuples of arity $\text{ar}(R)$, and v is a free tuple with $\text{vars}(v) \subseteq \text{vars}(\mathbf{T}) := \bigcup_{R \in \mathbf{S}} \text{vars}(\mathbf{T}(R))$. Accordingly, $\text{cons}(\mathbf{T}) := \bigcup_{R \in \mathbf{S}} \text{cons}(\mathbf{T}(R))$. For a query $q = (\mathbf{T}, v)$, we call **T** and v the query’s *tableau* and *answer tuple*, resp., and we let $\text{vars}(q) := \text{vars}(\mathbf{T})$ be the set of variables that occur in q . The *active domain* of q is the set $\text{adom}(q) := \text{cons}(v) \cup \text{cons}(\mathbf{T})$ of all constants in q .

Example 2.2. With this notation, query q_1 from Example 2.1 is the query (\mathbf{T}_1, v_1) with $v_1 = (Y_1)$ and $\mathbf{T}_1(\text{Person}) = \{(X_1, Y_1, Z_1)\}$, $\mathbf{T}_1(\text{Profession}) = \{(X_1, 'actor')\}$, $\mathbf{T}_1(\text{City}) = \{(Z_1, 'L.A.', 'U.S.')\}$.

We consider the *set semantics* of conjunctive queries, which is defined as follows. A *valuation* for a query q is a mapping $v: \text{vars}(q) \cup \mathbf{dom} \rightarrow \mathbf{dom}$ with $v(c) = c$ for every $c \in \mathbf{dom}$. For a free tuple $u = (u_1, \dots, u_r)$ of arity $r \geq 0$ we write $v(u)$ as a shorthand for $(v(u_1), \dots, v(u_r))$. An *embedding* of an **S**-CQ $q = (\mathbf{T}, v)$ into an **S**-db **I** is a valuation v for q such that for every $R \in \mathbf{S}$ and every free tuple $u \in \mathbf{T}(R)$ we have $v(u) \in \mathbf{I}(R)$. We write $\text{Emb}(q, \mathbf{I})$ for the set of all embeddings of q into **I**. The *query result* of $q = (\mathbf{T}, v)$ on **I** is the set $\llbracket q \rrbracket(\mathbf{I}) := \{v(v) : v \in \text{Emb}(q, \mathbf{I})\}$.

A *Boolean query* is an **S-CQ** $q = (\mathbf{T}, v)$ where v is the empty tuple $()$, i.e., the tuple of arity 0. The query result $\llbracket q \rrbracket(\mathbf{I})$ then is either the set $\{()\}$ or the empty set, corresponding to the answers “yes” and “no”, respectively. See Example 3.4 for two example queries.

Query Containment. For two queries q_1, q_2 of schema **S** we write $q_1 \sqsubseteq q_2$ and say that q_1 is *contained* in q_2 , if for all **S**-dbs **I** we have $\llbracket q_1 \rrbracket(\mathbf{I}) \subseteq \llbracket q_2 \rrbracket(\mathbf{I})$. We write $q_1 \not\sqsubseteq q_2$ to indicate that q_1 is *not* contained in q_2 (i.e., $\llbracket q_1 \rrbracket(\mathbf{I}) \not\subseteq \llbracket q_2 \rrbracket(\mathbf{I})$ for some **S**-db **I**).

Example 2.3. Consider the schema and query q_1 from Examples 2.1 and 2.2, and consider query

```
q2: SELECT DISTINCT A.pname
     FROM Person A, Profession B
     WHERE A.pid = B.pid
```

which is also taken from [9, Chapter 15]. In the syntax defined above, the query q_2 is the query (\mathbf{T}_2, v_2) with $v_2 = (Y_2)$ and $\mathbf{T}_2(\text{Person}) = \{(X_2, Y_2, Z_2)\}$, $\mathbf{T}_2(\text{Profession}) = \{(X_2, W_2)\}$, $\mathbf{T}_2(\text{City}) = \emptyset$.

By a close inspection of q_1 and q_2 , it is easy to see that q_2 is more general than q_1 , i.e., $\llbracket q_1 \rrbracket(\mathbf{I}) \subseteq \llbracket q_2 \rrbracket(\mathbf{I})$ holds for every database instance **I**. Thus, we have $q_1 \sqsubseteq q_2$. But there exist database instances **I** such that $\llbracket q_2 \rrbracket(\mathbf{I}) \not\subseteq \llbracket q_1 \rrbracket(\mathbf{I})$, and thus we have $q_2 \not\sqsubseteq q_1$.

Chandra and Merlin’s seminal paper [13] provided a characterization of query containment in terms of homomorphisms. To state their theorem, we need the following notation. Given a function $h: X \rightarrow Y$ (for some sets X and Y) and a k -tuple $v = (x_1, \dots, x_k) \in X^k$, we write $h(v)$ for the k -tuple $(h(x_1), \dots, h(x_k))$. For $S \subseteq X^k$ we let $h(S) := \{h(v) : v \in S\}$.

Definition 2.4. Let $q_1 = (\mathbf{T}_1, v_1)$ and $q_2 = (\mathbf{T}_2, v_2)$ be **S-CQs**, for some schema **S**. A *homomorphism* from q_2 to q_1 is a mapping $h: \text{vars}(q_2) \cup \text{adom}(q_2) \rightarrow \text{vars}(q_1) \cup \text{adom}(q_1)$ satisfying

- (1) $h(c) = c$, for every $c \in \text{adom}(q_2)$,
- (2) $h(v_2) = v_1$, and
- (3) for every $R \in \mathbf{S}$ and every $u \in \mathbf{T}_2(R)$ we have $h(u) \in \mathbf{T}_1(R)$.

THEOREM 2.5 (CHANDRA AND MERLIN’S HOMOMORPHISM THEOREM [13]). *For all schemas **S** and all **S-CQs** q_1 and q_2 we have $q_1 \sqsubseteq q_2 \iff$ there exists a homomorphism from q_2 to q_1 .*

Example 2.6. Consider the queries q_1, q_2 from Examples 2.2 and 2.3. Let $h: \{X_2, Y_2, Z_2, W_2\} \rightarrow \{X_1, Y_1, Z_1, \text{'actor'}, \text{'L.A.'}, \text{'U.S.'}\}$ be the mapping defined via $h(X_2) = X_1$, $h(Y_2) = Y_1$, $h(Z_2) = Z_1$, and $h(W_2) = \text{'actor'}$. It can easily be verified that h is a homomorphism from q_2 to q_1 (because $h(v_2) = h((Y_2)) = (h(Y_2)) = (Y_1) = v_1$ and $h((X_2, Y_2, Z_2)) = (X_1, Y_1, Z_1) \in \mathbf{T}_1(\text{Person})$ and $h((X_2, W_2)) = (X_1, \text{'actor'}) \in \mathbf{T}_1(\text{Profession})$). Theorem 2.5 yields that $q_1 \sqsubseteq q_2$. Yet there is no homomorphism from q_1 to q_2 , as $\mathbf{T}_1(\text{Profession})$ contains the tuple $(X_1, \text{'actor'})$, and any homomorphism h would have to map the constant ‘actor’ to itself, i.e., $h(\text{'actor'}) = \text{'actor'}$, but $\mathbf{T}_2(\text{Profession})$ does not contain any tuple with an entry ‘actor’ in its second component. Hence, Theorem 2.5 yields that $q_2 \not\sqsubseteq q_1$.

The *query containment problem for conjunctive queries* w.r.t. set semantics (QC-CQ) is the following decision problem: given a pair (q_1, q_2) of **S-CQs** (for some schema **S**), decide whether $q_1 \sqsubseteq q_2$.

By Theorem 2.5, QC-CQ can be solved by an algorithm that checks (e.g., by an exhaustive search) whether there is a homomorphism from q_2 to q_1 . This problem is NP-complete [13], even when inputs are restricted to Boolean queries and any fixed schema consisting of one (or several) relation(s) of arity 2.

Any algorithm that solves QC-CQ also yields an algorithm for checking if two queries q_1 and q_2 are *equivalent* – simply, by checking whether both $q_1 \sqsubseteq q_2$ and $q_2 \sqsubseteq q_1$ hold.

2.2 Quantum Computing & Simulated Annealing

This section is written from a non-physicist perspective and aims to provide an overview, giving sufficient information to database researchers for informed use of the concepts from quantum computing considered in this paper; more background can be found in Appendix A. Particular focus is put on quantum computing methods for solving optimization problems of the form

$$\bar{x} \in \arg \min_{\bar{x} \in C} p(\bar{x}). \quad (1)$$

Here, $p: \{0, 1\}^n \rightarrow \mathbb{R}$ is the *objective function*; it is a polynomial on n binary variables $\bar{x} = (x_1, \dots, x_n)$ with real-valued coefficients. The *search space* is the set $C \subseteq \{0, 1\}^n$. The goal is to find a tuple $\bar{x} \in C$ such that the value $p(\bar{x})$ is as small as possible. This optimization problem is called *unconstrained* if $C = \{0, 1\}^n$ and *constrained* if $C \subsetneq \{0, 1\}^n$. We write p as a sum of *monomials*, with each monomial being of the form $c \cdot \prod_{i=1}^n (x_i)^{j_i}$ where c is a real-valued coefficient, and j_i is a non-negative integer exponent associated with variable x_i (and, by convention, $(x_i)^0 = 1$). The *degree* of such a monomial is defined as the sum $\sum_{i=1}^n j_i$, and the degree of p is the maximum degree of its monomials. Since each variable x_i can only be assigned the values 0 and 1, and $0 \cdot 0 = 0$ and $1 \cdot 1 = 1$, any exponent $j_i \geq 1$ can be replaced with any positive integer j'_i without changing the function values of the polynomial. If the degree of p is ≤ 2 , we can assume without loss of generality that *every* monomial of p has degree exactly 2; this setting is known as *Quadratic Unconstrained Binary Optimization* problems (for short: QUBOs), cf. e.g. [22].

Quantum Approximate Optimization Algorithm for gate-based quantum computers. QAOA [18] is a hybrid quantum-classical algorithm designed for combinatorial optimization. It iteratively evaluates the objective function’s expected value for a parameter-dependent quantum state on a quantum processor, using classical feedback to update parameters and converge towards an optimal state. The quantum circuit consists of several *layers* that transition the system from the ground state of a so-called *mixing Hamiltonian* (describes the initial state) to that of the so-called *problem Hamiltonian* (describes the objective function). The problem solution is found by sampling the final state. Effectiveness is enhanced by incorporating problem constraints into the QAOA quantum circuit design [10, 52]. Then, only a subset of feasible solutions is explored, and the reduced size of the search space improves results.

The main complexity parameters of QAOA are the number of *layers* of the circuit, the number of *iterations* of the classical optimizer, and the number of *shots* performed to estimate the expected value of the objective function in each iteration.

The complexity of the quantum circuit depends on the specific problem constraints and the objective function p . In the following, we argue that the complexity scales polynomially in the number n of variables. This indicates that the problem can be efficiently executed on a quantum computer: For an arbitrary *quadratic* polynomial p of n binary variables $\bar{x} = (x_1, \dots, x_n)$ and the constraints considered in this work, the circuits for QAOA with ℓ layers have a favorable scaling of $O(\ell \cdot n^2)$ gates, $O(\ell \cdot n)$ depth (runtime), and

$O(n)$ qubits for both the constrained and unconstrained version [10, 52]. In general, for a fixed degree $d \leq n/2$ square-free polynomial p of n binary variables, the maximum number of monomials is $O(n^d)$ (practical instances are typically much sparser.). A degree d monomial requires $O(d)$ gates and circuit depth, and only a single ancilla qubit [27]. It follows that the circuits for QAOA with ℓ layers require $O(\ell \cdot d \cdot n^d)$ gates and depth, and $O(n)$ qubits, which is a polynomial scaling in the number of variables n . Hence, they can be efficiently executed on a quantum computer.

Currently available quantum hardware — referred to as Noisy Intermediate-Scale Quantum (NISQ) hardware — suffers from significant drawbacks: only a small number of physical qubits (e.g., up to 156 qubits on state-of-the-art IBM devices) are available, and computations are affected by limitations such as short coherence times that allow only shallow circuits to be run, and noise leading to gate and readout errors. Therefore, quantum algorithms currently are still mostly studied using simulators that run on classical hardware. In general, handling quantum states of n qubits requires storing and manipulating 2^n complex amplitudes, an exponential scaling that limits classical emulation to the small-scale regime. In practice, matrix product state simulators (e.g., provided by Qiskit Aer [26]) offer an efficient tool for approximately simulating quantum computations that rely on only a restricted amount of entanglement [46].

Simulated annealing and quantum annealing. Next, we present the foundations of two further methods that can be used to solve a QUBO, i.e., problem (1) (see above) in the *unconstrained* case where all monomials of p have *degree 2*. These methods are referred to as *simulated annealing* and *quantum annealing*. The term “annealing” is inspired by a cooling technique from metallurgy: heated metal is cooled in a controlled way such that its atoms have sufficient time to arrange themselves and form stable crystals. This results in a low-energy state of the metal that is considered to be stable. Both simulated annealing and quantum annealing are heuristic search methods moving in a controlled way over a so-called *solution landscape* or *energy landscape* (i.e., possible assignments of the binary variables; henceforth these are called *states*) for a sufficiently long time until they reach a stable and minimizing (w.r.t. the polynomial value) state. Thus, both methods contain the term “annealing” in their names. A minimum state corresponds to an optimal solution. In this work, we use three different solvers provided by the D-Wave library [6], which are briefly described in the following.

Simulated annealing. This solver emulates a controlled cooling procedure by considering a parameter β , which is related to a possible temperature T of a cooling process via $\beta = 1/(k_b \cdot T)$, where k_b denotes the Boltzmann constant. The cooling process is defined by a certain range for β limited by some β_{start} and β_{end} with $\beta_{\text{start}} \leq \beta \leq \beta_{\text{end}}$. Typically, one chooses for β_{start} a small value to start at a relatively high temperature, while β_{end} is large corresponding to a low temperature; β influences the probability of circumventing a barrier (value difference) in the energy landscape between neighboring states (i.e., states that differ in one bit). As β increases (i.e., T decreases), the probability of leaving a lower position decreases, such that the solver becomes less exploratory with time and finally terminates at a possible global minimum. Besides β , the difference between the values of neighboring states influences the probability of moving between them. In case of large positive

differences w.r.t. $1/\beta$, it is less likely that the solver leaves a current state. Otherwise, if there are negative differences, i.e. if the value of the neighboring state is lower, the current state will be left and the lower-valued neighbor will always be attained (cf., [35, Sec. 3.1]).

Quantum annealing. Contrary to simulated annealing, quantum annealing does not emulate a cooling process, but rather a controlled transfer from a quantum state that can be easily prepared to a quantum state that yields with high probability a global minimizer within a given energy landscape. This is done by introducing an annealing time t that ranges from 0 to some final time t_f . For a certain annealing time t , the quantum state is a weighted sum of the initial state and the final state. The weights in this sum are slowly adapted such that at the end of the annealing process, the final state is overweighted compared to the initial state (cf., [35, Sec. 3.2 & Chap. 4] and [38]). In contrast to simulated annealing, the probability of circumventing energy barriers for quantum annealing only depends on the width of the barrier (distance between states) rather than the height (difference between values).

Simulated quantum annealing. This solver is a classical version of quantum annealing, i.e. it emulates the behavior of a quantum annealer on a classical computer. The weights for the initial state and the final state are again determined by a parameter β , which is chosen in a similar way as in the case of simulated annealing [16].

Since only a finite number of betas and annealing times can be considered, the user has to provide a parameter denoted by *num_sweeps* (number of sweeps). As a result, the range for β and the annealing time are discretized by *num_sweeps* different values that are used within the annealing process. In addition to that, a *schedule* can be chosen to determine how β or the annealing time can be changed during an annealing process — either in a linear, or a geometric or a user-defined way. Since heuristic solution methods may not find a global minimizer after a single run, it might be required to run the solution method for multiple times. In D-Wave, one can fix the number of runs by providing an appropriate value for *num_reads* (number of reads). In terms of the solvers discussed above, a single run/read is equivalent to a single annealing process.

3 Optimization Problem for QC-CQ

This section’s aim is to translate an input instance (q_1, q_2) of the query containment problem QC-CQ into a triple (p, d, C) , where p is an integer-valued polynomial on binary variables, d is an integer, and C is a subset of the domain of p , such that the following is true:

$$\min_{\bar{x} \in C} p(\bar{x}) = d \iff q_1 \sqsubseteq q_2. \quad (2)$$

Notice that the minimization problem on the left-hand-side is similar to the one in equation (1); it can thus be solved using the methods described in Section 2.2. Concerning the right-hand-side, by Theorem 2.5, we can replace “ $q_1 \sqsubseteq q_2$ ” by “there exists a homomorphism from q_2 to q_1 ”. Recall that such a homomorphism is a mapping $h: A_2 \rightarrow A_1$, where $A_\ell = \text{vars}(q_\ell) \cup \text{adom}(q_\ell)$ for $\ell \in \{1, 2\}$, that satisfies conditions (1)–(3) of Definition 2.4.

In the following, we give a step-by-step description of how to construct the triple (p, d, C) for an input instance (q_1, q_2) of QC-CQ. Throughout this section, we let $q_1 = (\mathbf{T}_1, v_1)$ and $q_2 = (\mathbf{T}_2, v_2)$, and for $\ell \in \{1, 2\}$ we let $r_\ell = \text{ar}(v_\ell)$ and $v_\ell = (v_{\ell,1}, \dots, v_{\ell,r_\ell})$.

3.1 Preparation Step

The *preparation step* allows us to recognize certain cases that trivially violate query containment. We also establish some notation that will help us in the construction of the polynomial p .

Trivial violations of containment. The conditions of Definition 2.4 are obviously violated if (but not necessarily “only if”)

1. the answer tuples have different arities, i.e., $r_2 \neq r_1$ (then, condition (2) is violated), or
2. a constant in the answer tuple of q_2 would not be mapped to itself in the answer tuple of q_1 , i.e., there is a $k \leq r_2$ such that $v_{2,k} \in \mathbf{dom}$ and $v_{1,k} \neq v_{2,k}$ (then, satisfying condition (2) will violate condition (1)), or
3. the same variable appears more than once in the answer tuple of q_2 but would be mapped to different elements in the answer tuple of q_1 , i.e., there are $k, k' \leq r_2$ such that $v_{2,k} = v_{2,k'}$ but $v_{1,k} \neq v_{1,k'}$ (then, condition (2) is violated), or
4. the tableau of q_2 contains a non-empty relation that is empty in the tableau of q_1 , i.e., there is an $R \in \mathbf{S}$ such that $\mathbf{T}_2(R) \neq \emptyset = \mathbf{T}_1(R)$ (then, condition (3) is violated).

In each of these four cases, we can terminate and conclude that “ $q_1 \not\subseteq q_2$ ”. Otherwise, we proceed as described in the remainder of this section in order to construct the desired triple (p, d, C) .

Example 3.1. Let q_1, q_2 be the queries considered in the examples from Section 2.1. Upon input of the query pair (q_1, q_2) , none of the cases 1–4. apply, and we therefore will proceed as described in the rest of this section. But when exchanging the roles of q_1 and q_2 , the preparation step terminates and returns that $q_2 \not\subseteq q_1$, because case 4. applies since $\mathbf{T}_1(\text{City}) \neq \emptyset = \mathbf{T}_2(\text{City})$.

Bit-matrix. From now on, we assume that none of the cases 1–4. apply. Our goal is to construct a polynomial p on binary variables \bar{x} , an integer d and a set C such that Equivalence (2) holds.

The polynomial p will use binary variables of the form $x_{i,j}$ for $(i, j) \in A_2 \times A_1$, with $A_2 := \text{vars}(q_2) \cup \text{adom}(q_2)$ and $A_1 := \text{vars}(q_1) \cup \text{adom}(q_1)$. We view an *assignment* of the variables $x_{i,j}$ with values in $\{0, 1\}$ as a *bit-matrix* that can serve as a representation of a function $h: A_2 \rightarrow A_1$. Namely, h is represented by the *bit-matrix* $\bar{x} := (x_{i,j})_{(i,j) \in A_2 \times A_1}$ where, for all $i \in A_2$ and $j \in A_1$, we have $x_{i,j} \in \{0, 1\}$ and $x_{i,j} = 1 \iff h(i) = j$.

Example 3.2. Consider queries q_1, q_2 and homomorphism h from Example 2.6. We have $A_2 = \{X_2, Y_2, Z_2, W_2\}$ and $A_1 = \{X_1, Y_1, Z_1, \text{'actor'}, \text{'L.A.'}, \text{'U.S.'}\}$. The bit-matrix representation of h is:

$$\begin{array}{c} X_2 \\ Y_2 \\ Z_2 \\ W_2 \end{array} \begin{pmatrix} X_1 & Y_1 & Z_1 & \text{'actor'} & \text{'L.A.'} & \text{'U.S.'} \\ \left(\begin{array}{cccccc} 1 & 0 & 0 & 0 & 0 & 0 \\ 0 & 1 & 0 & 0 & 0 & 0 \\ 0 & 0 & 1 & 0 & 0 & 0 \\ 0 & 0 & 0 & 1 & 0 & 0 \end{array} \right) \end{pmatrix}$$

E.g., the entry in row X_2 and column X_1 is addressed as the bit $x_{i,j}$ with $i = X_2$ and $j = X_1$; in the above matrix, this bit is set to 1.

Note that a bit-matrix $\bar{x} \in \{0, 1\}^{A_2 \times A_1}$ represents a mapping from A_2 to A_1 if, and only if, for every $i \in A_2$ there is exactly one $j \in A_1$ with $x_{i,j} = 1$ (i.e., exactly one bit per matrix row is 1).

Next, we make use of the fact that we already know that the query pair (q_1, q_2) satisfies none of the cases 1–4. We can restrict our attention to mappings $h: A_2 \rightarrow A_1$ where $h(v_{2,k}) = v_{1,k}$ for every $k \leq r_2$. Furthermore, condition (1) in Definition 2.4 demands that

$h(c) = c$ for all $c \in \text{adom}(q_2)$. Thus, the values of h are predefined on all elements in $\text{adom}(q_2) \cup \text{vars}(v_2)$. Therefore, instead of A_2 , we only consider $B_2 := A_2 \setminus (\text{adom}(q_2) \cup \text{vars}(v_2))$, and we extend any bit-matrix $\bar{x} \in \{0, 1\}^{B_2 \times A_1}$ to a bit-matrix $\bar{x}^{(e)} \in \{0, 1\}^{A_2 \times A_1}$ by letting $x_{i,j}^{(e)} = x_{i,j}$ for all $(i, j) \in B_2 \times A_1$ and

- (a) for all $c \in \text{adom}(q_2)$ and $j \in A_1$ we let $x_{c,j}^{(e)} = 1 \iff j = c$,
- (b) for all $i \in \text{vars}(v_2)$ and $j \in A_1$ we let $x_{i,j}^{(e)} = 1 \iff$ there is a $k \leq r_2$ with $i = v_{2,k}$ and $j = v_{1,k}$.

This ensures that if $\bar{x}^{(e)}$ represents some mapping $h: A_2 \rightarrow A_1$, then this mapping satisfies the conditions (1) and (2) of Definition 2.4.

We use the same notation when considering the *binary variables* $\bar{x} = (x_{i,j})_{(i,j) \in B_2 \times A_1}$ and write $\bar{x}^{(e)}$ for the matrix obtained by extending the variable-matrix \bar{x} with additional rows i for all $i \in \text{adom}(q_2) \cup \text{vars}(v_2)$; each additional row is already filled with elements from $\{0, 1\}$, defined as in the above items (a) and (b).

Example 3.3. Recall from Example 3.2 the particular sets A_2 and A_1 . Note that $\text{adom}(q_2) = \emptyset$ and $\text{vars}(v_2) = \{Y_2\}$. Hence, $B_2 = A_2 \setminus \{Y_2\} = \{X_2, Z_2, W_2\}$. We will use binary variables $x_{i,j}$ for $(i, j) \in B_2 \times A_1$. I.e., we consider the variable-matrix $\bar{x} = (x_{i,j})_{(i,j) \in B_2 \times A_1}$. The extension $\bar{x}^{(e)}$ of \bar{x} is obtained by adding a row for Y_2 (since $\text{adom}(q_2) \cup \text{vars}(v_2) = \{Y_2\}$). This yields the matrix $\bar{x}^{(e)} =$

$$\begin{array}{c} X_2 \\ Y_2 \\ Z_2 \\ W_2 \end{array} \begin{pmatrix} X_1 & Y_1 & Z_1 & \text{'actor'} & \text{'L.A.'} & \text{'U.S.'} \\ \left(\begin{array}{cccccc} x_{X_2, X_1} & x_{X_2, Y_1} & x_{X_2, Z_1} & x_{X_2, \text{'actor'}} & x_{X_2, \text{'L.A.}} & x_{X_2, \text{'U.S.}} \\ 0 & 1 & 0 & 0 & 0 & 0 \\ x_{Z_2, X_1} & x_{Z_2, Y_1} & x_{Z_2, Z_1} & x_{Z_2, \text{'actor'}} & x_{Z_2, \text{'L.A.}} & x_{Z_2, \text{'U.S.}} \\ x_{W_2, X_1} & x_{W_2, Y_1} & x_{W_2, Z_1} & x_{W_2, \text{'actor'}} & x_{W_2, \text{'L.A.}} & x_{W_2, \text{'U.S.}} \end{array} \right) \end{pmatrix}$$

This reflects that the answer tuples of q_2 and q_1 are (Y_2) and (Y_1) , and any homomorphism from q_2 to q_1 must map Y_2 to Y_1 .

As a result of the preparation step upon input of an arbitrary query pair (q_1, q_2) , we either output that $q_1 \not\subseteq q_2$ or we output the sets A_2, B_2, A_1 and the variable-matrix \bar{x} and its extension $\bar{x}^{(e)}$. In the next subsection, we explain how these are used to define a triple (p, d, C) that satisfies Equivalence (2). Polynomial p will use the binary variables \bar{x} and will also utilize the additional 0-1-entries in the extended matrix $\bar{x}^{(e)}$. Yet first, let us consider another example.

Example 3.4. We consider directed graphs in a relational encoding. Accordingly, let \mathbf{S}_g be the schema consisting of a binary relation name E , for representing the edges of a graph.

Consider the Boolean queries “2-cycle” $q_{2cy} := (\mathbf{T}_{2cy}, v_{2cy})$ and “2-chain” $q_{2ch} := (\mathbf{T}_{2ch}, v_{2ch})$ defined via $v_{2cy} = v_{2ch} = ()$ and $\mathbf{T}_{2cy}(E) = \{(Z, Z'), (Z', Z)\}$ and $\mathbf{T}_{2ch}(E) = \{(Z, Z_1), (Z_1, Z_2)\}$. An \mathbf{S}_g -db D represents a directed graph, and $q_{2cy}(D) = \text{“yes”}$ iff this graph contains a directed cycle on at most 2 nodes, while $q_{2ch}(D) = \text{“yes”}$ iff this graph contains a directed path of length 2. Upon input of the query pair (q_{2cy}, q_{2ch}) , the preparation step yields $A_2 = B_2 = \{Z_0, Z_1, Z_2\}$, $A_1 = \{Z, Z'\}$, and \bar{x} consists of the binary variables $x_{i,j}$ for all $(i, j) \in B_2 \times A_1$. Since $A_2 = B_2$, we have $\bar{x}^{(e)} = \bar{x}$, i.e., no additional rows with 0-1-entries are inserted into \bar{x} .

3.2 Generic choice of (p, d, C)

In our generic choice of (p, d, C) we let $C = \{0, 1\}^{B_2 \times A_1}$. Our goal is to define d and p in such a way that Equivalence (2) holds. Here, p will be an integer-valued polynomial on the binary variables $\bar{x} = (x_{i,j})_{(i,j) \in B_2 \times A_1}$; we will define p in such a way, that for an

assignment $\bar{x} \in \{0, 1\}^{B_2 \times A_1}$ of the binary variables with actual bits, the following is true: the value $p(\bar{x})$ is minimal and equal to $d \iff$ the extended bit-matrix $\bar{x}^{(e)}$ represents a function $h: A_2 \rightarrow A_1$ that, in fact, is a homomorphism from q_2 to q_1 .

For defining p , we will use a number of intermediate polynomials that are introduced in the following. The first of these is

$$p_{\text{fct}}(\bar{x}) := \sum_{i \in B_2} \sum_{\substack{j, j' \in A_1 \\ j < j'}} (x_{i,j} \cdot x_{i,j'}).$$

Here, $<$ denotes an arbitrary linear order on A_1 (which corresponds to the arrangement of the columns in the variable-matrix \bar{x}). When assigning the binary variables in \bar{x} to actual bits in $\{0, 1\}$, this polynomial evaluates to an integer ≥ 0 ; and it evaluates to exactly 0 if, and only if, in every row $i \in B_2$ there is at most one column $j \in A_1$ such that the variable $x_{i,j}$ is assigned the value 1. Hence, if it evaluates to a value > 0 , then the assigned bit-matrix (and its extension) for sure does *not* represent any function $h: A_2 \rightarrow A_1$, let alone an actual homomorphism from q_2 to q_1 .

Example 3.5. Continuing Example 3.4, we have $p_{\text{fct}}(\bar{x}) = (x_{Z_0,Z} \cdot x_{Z_0,Z'}) + (x_{Z_1,Z} \cdot x_{Z_1,Z'}) + (x_{Z_2,Z} \cdot x_{Z_2,Z'})$.

Next, we introduce several polynomials that will help us handle condition (3) of Definition 2.4. Consider a relation $R \in \mathbf{S}$ and a tuple $u \in \mathbf{T}_2(R)$. Let $r = \text{ar}(u)$ and $(u_1, \dots, u_r) = u$, and note that $\{u_1, \dots, u_r\} \subseteq A_2 = B_2 \cup \text{adom}(q_2) \cup \text{vars}(v_2)$. Recall that \bar{x} is a variable-matrix that contains a row i for every $i \in B_2$; and $\bar{x}^{(e)}$ extends \bar{x} by additional rows for every $i \in \text{adom}(q_2) \cup \text{vars}(v_2)$, and these rows are already filled with 0-1-entries. We define

$$p_{R,u}(\bar{x}) := \sum_{(w_1, \dots, w_r) \in \mathbf{T}_1(R)} \left(- \prod_{k=1}^r x_{u_k, w_k}^{(e)} \right).$$

Since $x_{u_k, w_k}^{(e)}$ will be assigned with values in $\{0, 1\}$, the product will evaluate to either 0 or 1. By a close inspection of the polynomial, we can prove (cf. Appendix B):

LEMMA 3.6. *For all $R \in \mathbf{S}$, $u \in \mathbf{T}_2(R)$, $\bar{x} \in \{0, 1\}^{B_2 \times A_1}$ we have*

- (a) $p_{R,u}(\bar{x})$ is an integer with $-|\mathbf{T}_1(R)| \leq p_{R,u}(\bar{x}) \leq 0$, and
- (b) if $p_{\text{fct}}(\bar{x}) = 0$ then $p_{R,u}(\bar{x}) \in \{-1, 0\}$ and, moreover, $p_{R,u}(\bar{x}) = -1 \iff$ for the extended bit-matrix $\bar{x}^{(e)}$ associated with \bar{x} and letting $r = \text{ar}(R)$ and $(u_1, \dots, u_r) = u$, for every $k \leq r$ we have $\sum_{z \in A_1} x_{u_k, z}^{(e)} = 1$, and letting z_k be the particular $z \in A_1$ with $x_{u_k, z}^{(e)} = 1$ we have $(z_1, \dots, z_r) \in \mathbf{T}_1(R)$.

Part (b) of this lemma tells us that if the binary variables are assigned with 0-1-values such that at most one bit per matrix row is 1, then the following is true: $p_{R,u}(\bar{x})$ evaluates to $-1 \iff$ for every entry u_k of u , the row u_k of $\bar{x}^{(e)}$ contains exactly one 1, and for the particular column z_k that carries this 1, the tuple (z_1, \dots, z_r) belongs to the tableau $\mathbf{T}_1(R)$. The latter can serve as a witness that condition (3) of Definition 2.4 is satisfied. Condition (3) demands that this holds for all relations $R \in \mathbf{S}$ and all $u \in \mathbf{T}_2(R)$; and accordingly, we define the polynomial

$$p_{(3)}(\bar{x}) := \sum_{R \in \mathbf{S}} \sum_{u \in \mathbf{T}_2(R)} p_{R,u}(\bar{x}).$$

Example 3.7. Consider the query pair $(p_{2\text{cy}}, p_{2\text{ch}})$ from Examples 3.4 and 3.5. The tuple $(Z_0, Z_1) \in \mathbf{T}_{2\text{ch}}(E)$ yields $p_{E, (Z_0, Z_1)}(\bar{x}) = -x_{Z_0,Z} \cdot x_{Z_1,Z'} - x_{Z_0,Z'} \cdot x_{Z_1,Z}$; the tuple $(Z_1, Z_2) \in \mathbf{T}_{2\text{ch}}(E)$ yields

$p_{E, (Z_1, Z_2)}(\bar{x}) = -x_{Z_1,Z} \cdot x_{Z_2,Z'} - x_{Z_1,Z'} \cdot x_{Z_2,Z}$; and in summary we have $p_{(3)}(\bar{x}) = p_{E, (Z_0, Z_1)}(\bar{x}) + p_{E, (Z_1, Z_2)}(\bar{x}) = -x_{Z_0,Z} \cdot x_{Z_1,Z'} - x_{Z_0,Z'} \cdot x_{Z_1,Z} - x_{Z_1,Z} \cdot x_{Z_2,Z'} - x_{Z_1,Z'} \cdot x_{Z_2,Z}$.

For each $i \in \{1, 2\}$ we let $|\mathbf{T}_i| := \sum_{R \in \mathbf{S}} |\mathbf{T}_i(R)|$. Using Lemma 3.6, we can prove the following (cf. Appendix B):

LEMMA 3.8. *For every $\bar{x} \in \{0, 1\}^{B_2 \times A_1}$ we have:*

- (a) $p_{(3)}(\bar{x})$ is an integer with $-\sum_{R \in \mathbf{S}} |\mathbf{T}_1(R)| \cdot |\mathbf{T}_2(R)| \leq p_{(3)}(\bar{x}) \leq 0$.
- (b) If $p_{\text{fct}}(\bar{x}) = 0$ then $-|\mathbf{T}_2| \leq p_{(3)}(\bar{x}) \leq 0$ and, moreover, $p_{(3)}(\bar{x}) = -|\mathbf{T}_2| \iff$ the extended bit-matrix $\bar{x}^{(e)}$ associated with \bar{x} satisfies the following: for every $i \in A_2$ we have $\sum_{j \in A_1} x_{i,j}^{(e)} = 1$, i.e., $\bar{x}^{(e)}$ represents a mapping $h: A_2 \rightarrow A_1$ via $h(i) = j$ iff $x_{i,j}^{(e)} = 1$, and this mapping is a homomorphism from q_2 to q_1 .

Part (b) tells us that if the binary variables are assigned with 0-1-values such that at most one bit per matrix row is 1, then we have: $p_{(3)}(\bar{x})$ evaluates to $-|\mathbf{T}_2| \iff$ the extended bit-matrix $\bar{x}^{(e)}$ associated with \bar{x} represents a mapping $h: A_2 \rightarrow A_1$ that, in fact, is a homomorphism from q_2 to q_1 . This leads us to define

$$p_{\text{gen}}(\bar{x}) := p_{(3)}(\bar{x}) + (|\mathbf{T}_1| \cdot |\mathbf{T}_2| + 1) \cdot p_{\text{fct}}(\bar{x}).$$

If \bar{x} is an assignment with 0-1-values such that $p_{\text{fct}}(\bar{x}) = 0$, then we obtain from Lemma 3.8 that $p_{\text{gen}}(\bar{x})$ is an integer between $-|\mathbf{T}_2|$ and 0; and it is exactly $-|\mathbf{T}_2|$ iff the extended bit-matrix $\bar{x}^{(e)}$ represents a homomorphism from q_2 to q_1 (witnessing that $q_1 \sqsubseteq q_2$). On the other hand, for any assignment \bar{x} with $p_{\text{fct}}(\bar{x}) \neq 0$ we have $p_{\text{fct}}(\bar{x}) \geq 1$, and thus $p_{\text{gen}}(\bar{x}) \geq 0$. Actually, the same still holds if in the definition of $p_{\text{gen}}(\bar{x})$ we replace the term “ $|\mathbf{T}_1| \cdot |\mathbf{T}_2|$ ” with any number $\geq \sum_{R \in \mathbf{S}} |\mathbf{T}_1(R)| \cdot |\mathbf{T}_2(R)|$.

In our generic choice for (p, d, C) , we let $p(\bar{x}) := p_{\text{gen}}(\bar{x})$, $d := d_{\text{gen}} = -|\mathbf{T}_2|$ and $C := C_{\text{gen}} = \{0, 1\}^{B_2 \times A_1}$. The following theorem states that this choice is correct; the theorem’s proof (cf. Appendix B) relies on Lemma 3.8 and Theorem 2.5.

THEOREM 3.9. *Let $(p, d, C) := (p_{\text{gen}}, d_{\text{gen}}, C_{\text{gen}})$.*

For every $\bar{x} \in C$ we have $p(\bar{x}) \geq d$. Furthermore, $\min_{\bar{x} \in C} p(\bar{x}) = d \iff q_1 \sqsubseteq q_2$. Moreover, for every $\bar{x} \in C$ with $p(\bar{x}) = d$, the extended bit-matrix $\bar{x}^{(e)}$ represents a homomorphism from q_2 to q_1 .

This theorem tells us that in order to decide whether $q_1 \sqsubseteq q_2$, we can seek for a bit-matrix $\bar{x}^* \in C_{\text{gen}}$ such that $p_{\text{gen}}(\bar{x}^*)$ is as small as possible. If $p_{\text{gen}}(\bar{x}^*) = d_{\text{gen}}$, then we know that $q_1 \sqsubseteq q_2$ and, moreover, \bar{x}^* represents a homomorphism from q_2 to q_1 and can thus serve as a certificate which proves that $q_1 \sqsubseteq q_2$. Otherwise, $p_{\text{gen}}(\bar{x}^*) > d_{\text{gen}}$, and we know that $q_1 \not\sqsubseteq q_2$.

In Sections 4 & 5 we present a quantum computing solution for finding \bar{x}^* . The size of the search space is $|C_{\text{gen}}| = 2^{n_2 \cdot n_1}$ for $n_2 := |B_2|$ and $n_1 := |A_1|$. The number of qubits (and thus, the computational resources) required for our solution is closely related to the number of binary variables present in the polynomial $p_{\text{gen}}(\bar{x})$. The number of binary variables occurring in $p_{\text{gen}}(\bar{x})$ is $n_2 \cdot n_1 = |B_2| \cdot |A_1|$. The next two subsections present optional modifications that may decrease the number of binary variables and the size of the search space.

Example 3.10. Consider the query pair $(p_{2\text{cy}}, p_{2\text{ch}})$ from Example 3.4 and recall the polynomials $p_{\text{fct}}(\bar{x})$ and $p_{(3)}(\bar{x})$ constructed in Examples 3.5 & 3.7. Then, $|\mathbf{T}_{2\text{cy}}| \cdot |\mathbf{T}_{2\text{ch}}| + 1 = 2 \cdot 2 + 1 = 5$ and

$p_{gen}(\bar{x}) = p_{(3)}(\bar{x}) + 5 \cdot p_{fct}(\bar{x})$. Furthermore, $d_{gen} = -|\mathbf{T}_{2ch}| = -2$ and $C_{gen} = \{0, 1\}^{B_2 \times A_1}$ for $B_2 = \{Z_0, Z_1, Z_2\}$ and $A_1 = \{Z, Z'\}$.

3.3 Simplification Step

This section presents an optional *simplification step* that closely inspects the polynomial $p_{(3)}(\bar{x})$ with the aim of restricting B_2 to a subset $B_2^{(s)}$, so that the total number of binary variables is reduced from $n_2 \cdot n_1$ to $n_2^{(s)} \cdot n_1$ for $n_2^{(s)} = |B_2^{(s)}|$. In the following, we describe a process that starts with $B_2^{(s)} := B_2$ and $\bar{x}^{(s)} := \bar{x}^{(e)}$, and that iteratively removes elements from $B_2^{(s)}$ and adapts $\bar{x}^{(s)}$ accordingly.

The idea is that for tuples in q_2 that have only one tuple in q_1 to which they can fit, we can already map the variables of that tuple accordingly. Moreover, if no tuple in q_1 fits (e.g. due to fixed mappings already found during the preparation step), then we can already conclude that $q_1 \not\subseteq q_2$. Following this idea, we iteratively check all tuples in q_2 for potential simplifications.

By definition, $p_{(3)}(\bar{x}) = \sum_{R \in \mathbf{S}} \sum_{u \in \mathbf{T}_2(R)} p_{R,u}(\bar{x})$, for

$$p_{R,u}(\bar{x}) = \sum_{(w_1, \dots, w_r) \in \mathbf{T}_1(R)} \left(- \prod_{k=1}^r x_{u_k, w_k}^{(e)} \right),$$

where $(u_1, \dots, u_r) = u$. Here, $x_{u_k, w_k}^{(e)}$ is the binary variable x_{u_k, w_k} if $u_k \in B_2$, and it is a fixed 0-1-value if $u_k \in A_2 \setminus B_2$. In particular, if there is a k with $u_k \in A_2 \setminus B_2$ and $x_{u_k, w_k}^{(e)} = 0$, then the entire product $\prod_{k=1}^r x_{u_k, w_k}^{(e)}$ evaluates to 0, and hence the tuple $(w_1, \dots, w_r) \in \mathbf{T}_1(R)$ has zero contribution in the polynomial $p_{R,u}(\bar{x})$.

If every $w \in \mathbf{T}_1(R)$ has zero contribution, $p_{R,u}(\bar{x})$ is the constant polynomial 0. From Lemma 3.8 we obtain that there does not exist any homomorphism from q_2 to q_1 ; we stop and output “ $q_1 \not\subseteq q_2$ ”.

If there is exactly one $w = (w_1, \dots, w_r) \in \mathbf{T}_1(R)$ that does not have zero contribution, then $p_{R,u}(\bar{x}) = - \prod_{k=1}^r x_{u_k, w_k}^{(e)}$. From Lemma 3.8 we then obtain that if there exists a homomorphism h from q_2 to q_1 , then it must satisfy $h(u_k) = w_k$ for all $k \leq r$. We can therefore treat the tuples u and w in a similar way as we had treated the queries' answer tuples v_2 and v_1 in the preparation step: If there are $k, k' \leq r$ such that $u_k = u_{k'}$ but $w_k \neq w_{k'}$, then we know that there does not exist any homomorphism from q_2 to q_1 , and hence we can stop and output “ $q_1 \not\subseteq q_2$ ”. Similarly, if there is a $k \leq r$ such that $u_k \notin B_2^{(s)}$ and $x_{u_k, w_k}^{(e)} = 0$, we know that some previously considered constraint had demanded that $h(u_k) \neq w_k$ while the currently considered constraint demands that $h(u_k) = w_k$; hence, we can stop and output “ $q_1 \not\subseteq q_2$ ”. Otherwise, we remove u_1, \dots, u_r from $B_2^{(s)}$ and modify the definition of $\bar{x}^{(s)}$ by setting $x_{u_k, w_k}^{(s)} := 1$ and $x_{u_k, j}^{(s)} := 0$ for all $j \in A_1 \setminus \{w_k\}$ and all $k \leq r$.

We loop through all $R \in \mathbf{S}$ and all $u \in \mathbf{T}_2(R)$ and apply this procedure. We use the resulting matrix $\bar{x}^{(s)}$ and the set $B_2^{(s)}$ and let $n_2^{(s)} := |B_2^{(s)}|$. Our *simplified choice* of (p, d, C) , which we denote as $(p_{sim}, d_{sim}, C_{sim})$, is defined via $C_{sim} = \{0, 1\}^{B_2^{(s)} \times A_1}$, $d_{sim} = -|\mathbf{T}_2|$, and $p_{sim}(\bar{x})$ is the polynomial on binary variables $x_{i,j}$ for $(i, j) \in B_2^{(s)} \times A_1$ with $p_{sim}(\bar{x}) := p_{(3)}^{(s)}(\bar{x}) + (|\mathbf{T}_1| \cdot |\mathbf{T}_2| + 1) \cdot p_{fct}^{(s)}(\bar{x})$, where $p_{(3)}^{(s)}(\bar{x})$ is defined in the same way as $p_{(3)}(\bar{x})$, but $x_{u_k, w_k}^{(e)}$ is replaced by $x_{u_k, w_k}^{(s)}$, and $p_{fct}^{(s)}(\bar{x})$ is defined as $p_{fct}(\bar{x})$, but the leftmost sum

runs only over $i \in B_2^{(s)}$. Using Theorem 3.9, the construction of $(p_{sim}, d_{sim}, C_{sim})$ immediately yields:

THEOREM 3.11. *The statement of Theorem 3.9 holds for $(p, d, C) := (p_{sim}, d_{sim}, C_{sim})$ when replacing $\bar{x}^{(e)}$ with $\bar{x}^{(s)}$.*

The number of binary variables occurring in the polynomial $p_{sim}(\bar{x})$ is $n_2^{(s)} \cdot n_1$, where $n_2^{(s)} := |B_2^{(s)}| \leq n_2$.

Example 3.12. When considering the query pair (p_{2cy}, p_{2ch}) from Examples 3.4, 3.5, 3.7, 3.10, we have $A_2 \setminus B_2 = \emptyset$ and $|\mathbf{T}_{2cy}(E)| > 1$, and hence the simplification step does not change anything and we obtain $B_2^{(s)} = B_2$ and $(p_{sim}, d_{sim}, C_{sim}) = (p_{gen}, d_{gen}, C_{gen})$.

Example 3.13. When considering the query pair (q_1, q_2) from Examples 2.2, 2.3, 3.3, recall that $B_2 = \{X_2, Z_2, W_2\}$ and $A_2 \setminus B_2 = \{Y_2\}$ and $x_{Y_2, Y_1}^{(e)} = 1$ and $x_{Y_2, j}^{(e)} = 0$ for every $j \in A_1 \setminus \{Y_2\}$. We have

$$\begin{aligned} p_{(3)}(\bar{x}) &= p_{\text{Person}, (X_2, Y_2, Z_2)}(\bar{x}) + p_{\text{Profession}, (X_2, W_2)}(\bar{x}) \\ &= -x_{X_2, X_1}^{(e)} \cdot x_{Y_2, Y_1}^{(e)} \cdot x_{Z_2, Z_1}^{(e)} - x_{X_2, X_1}^{(e)} \cdot x_{W_2, \text{actor}}^{(e)} \\ &= -x_{X_2, X_1} \cdot 1 \cdot x_{Z_2, Z_1} - x_{X_2, X_1} \cdot x_{W_2, \text{actor}}. \end{aligned}$$

During simplification, we initialize $B_2^{(s)}$ to B_2 and then remove from $B_2^{(s)}$ the variables X_2, Z_2 , and let $x_{X_2, X_1}^{(s)} = 1$, $x_{Z_2, Z_1}^{(s)} = 1$, $x_{X_2, j}^{(s)} = 0$ for all $j \in A_1 \setminus \{X_1\}$ and $x_{Z_2, j}^{(s)} = 0$ for all $j \in A_1 \setminus \{Z_1\}$.

Afterwards, we remove W_2 from $B_2^{(s)}$ and let $x_{W_2, \text{actor}}^{(s)} = 1$ and $x_{W_2, j}^{(s)} = 0$ for all $j \in A_1 \setminus \{\text{actor}\}$. Then, $B_2^{(s)} = \emptyset$ and $p_{(3)}^{(s)}(\bar{x}) = -x_{X_2, X_1}^{(s)} \cdot x_{Z_2, Z_1}^{(s)} - x_{X_2, X_1}^{(s)} \cdot x_{W_2, \text{actor}}^{(s)} = -2$ and $p_{fct}^{(s)}(\bar{x}) = 0$. Thus, we obtain: $p_{sim}(\bar{x}) = -2$, $d_{sim} = -|\mathbf{T}_2| = -2$, and $C_{sim} = \{0, 1\}^{\emptyset \times A_1}$ which, by convention, is the set $\{\emptyset\}$ consisting only of the empty tuple $()$. We leverage this in Example 3.15.

3.4 Using Constraints

A further optional step is to *use constraints*, i.e., to restrict the set C of considered bit-matrices \bar{x} to those bit-matrices that actually represent functions (i.e. where there is exactly one 1 per row). Such constraints can be imposed using an adapted QAOA version as explained in Section 2.2. This drastically reduces the search space, and additionally, it allows to simplify the polynomial $p(\bar{x})$ by completely dropping the term involving $p_{fct}(\bar{x})$. Accordingly, for our choices $(p_{gen}, d_{gen}, C_{gen})$ and $(p_{sim}, d_{sim}, C_{sim})$, we get new *constrained* versions $(p_{gen}^c, d_{gen}^c, C_{gen}^c)$ and $(p_{sim}^c, d_{sim}^c, C_{sim}^c)$, which are defined as follows: $p_{gen}^c(\bar{x}) := p_{(3)}(\bar{x})$, $p_{sim}^c(\bar{x}) := p_{(3)}^{(s)}(\bar{x})$, $d_{gen}^c := d_{gen} = -|\mathbf{T}_2|$, $d_{sim}^c := d_{sim} = -|\mathbf{T}_2|$, and C_{gen}^c is the set of all bit-matrices $\bar{x} \in \{0, 1\}^{B_2 \times A_1}$ where for all $i \in B_2$ there is exactly one $j \in A_1$ with $x_{i,j} = 1$, while C_{sim}^c is defined analogously, by replacing B_2 with $B_2^{(s)}$. Note that $|C_{gen}^c| = (n_1)^{n_2} \leq |C_{gen}| = 2^{n_2 \cdot n_1}$ and $|C_{sim}^c| = (n_1)^{n_2^{(s)}} \leq |C_{sim}| = 2^{n_2^{(s)} \cdot n_1}$. Theorems 3.9 and 3.11 yield:

COROLLARY 3.14.

The statement of Theorem 3.9 holds for $(p, d, C) := (p_{gen}^c, d_{gen}^c, C_{gen}^c)$. The statement of Theorem 3.11 holds for $(p, d, C) := (p_{sim}^c, d_{sim}^c, C_{sim}^c)$.

3.5 Identifying Trivial Cases

Let (p, d, C) be any of the choices $(p_{gen}, d_{gen}, C_{gen})$, $(p_{gen}^c, d_{gen}^c, C_{gen}^c)$, $(p_{sim}, d_{sim}, C_{sim})$, $(p_{sim}^c, d_{sim}^c, C_{sim}^c)$. If the polynomial p actually does

not contain any binary variable (e.g. if all variables have been assigned during preparation and/or simplification; see Appendix B for details), then $p(\bar{x})$ is the constant function ℓ , for some integer ℓ (for short: $p(\bar{x}) \equiv \ell$). In case $p(\bar{x}) \equiv \ell$ for an integer ℓ , we obtain from Theorems 3.9 and 3.11, and Corollary 3.14, that $q_1 \not\sqsubseteq q_2$ if $\ell \neq d$, and $q_1 \sqsubseteq q_2$ if $\ell = d$; in the latter case we can construct a homomorphism from q_2 to q_1 as a certificate proving $q_1 \sqsubseteq q_2$.

Example 3.15. We continue Example 3.13 and consider the choice $(p_{sim}, d_{sim}, C_{sim})$. Recall that $p_{sim}(\bar{x}) \equiv -2$ and $d_{sim} = -2$. As explained above, this constitutes a trivial case where we can stop and output “ $q_1 \sqsubseteq q_2$ ”. Inspecting the definition of $\bar{x}^{(s)}$ yields a homomorphism from q_2 to q_1 , namely the mapping $h: A_2 \rightarrow A_1$ with $h(X_2) = X_1$, $h(Y_2) = Y_1$, $h(Z_2) = Z_1$, and $h(W_2) = \text{‘actor’}$.

Recall that during preparation and simplification, we have also identified trivial cases in which we can stop and output “ $q_1 \not\sqsubseteq q_2$ ”.

4 System and Workflow

Figure 2 shows our 3-stage workflow. The *preprocessing stage* translates the input, a pair of conjunctive queries, into a polynomial. First is the preparation step (①), as described in Section 3.1, which can detect certain trivial cases. Simplification (②) and the addition of constraints (③) are optional, and either combination can result in different polynomials. Trivial problems (④) are answered directly.

Next is the decision whether to use QAOA or annealing in the *quantum stage*. If the problem is constrained or has a degree higher than two, the system defaults to QAOA (steps ⑤ and ⑥). In all other cases, the system follows the user’s preference (⑦). Our solvers can be either simulator software, or quantum devices (⑧). Software libraries (from Qrisp and D-Wave) provide access to solvers (Appendix C provides architectural details).

Performing several measurements, we obtain a set of bitvectors, where each encodes a bit-matrix.

In *postprocessing*, we check each bitvector \bar{x} in polynomial time for validity and optimality: We check whether the bitvector represents a bit-matrix with at most one 1 per row (validity), and we compute the function value $p(\bar{x})$ and compare it to the known optimal value (optimality). Despite the theoretical correctness, the additional validity check is necessary for constrained QAOA on real hardware, due to potential hardware errors and noise. Invalid results are directly discarded. Each valid and optimal bitvector can be interpreted as a homomorphism certifying query containment (⑨). If no such bitvector is found, the system reports that containment does not hold.

5 Experiments

We explore the following research questions. To not be limited by current hardware, we rely on simulators for the first three.

- RQ1: Soundness: Can our approach correctly solve QC-CQ?
- RQ2: Scalability: How does the probability of solving QC-CQ problems scale with the size of these problems?
- RQ3: Parameter sensitivity: How do QAOA-specific parameters affect the probability of solving QC-CQ?
- RQ4: Feasibility on current hardware: Can we successfully demonstrate a proof-of-concept on current quantum hardware?

5.1 Metrics

Experiments with *positive* and *negative* query pairs (containment holds or does not hold) allow to capture *classification outcomes* (true/false positives/negatives). Since our approach produces a certificate, it cannot produce any false positives.

We determine how likely it is to successfully solve a QC-CQ problem and track the *solution probability* as the fraction of *measurements* (reads for annealing, shots for QAOA) for which an optimal solution is found. Here, we only consider positive query pairs, as the solution probability of negative pairs is always 100%. As long as the solution probability is non-zero, we find a certifying homomorphism which proves that containment holds.¹

5.2 Experimental Setup

Query Pairs. We manually extracted query pairs from textbooks and benchmarks. Thus, these “*T&B problems*” are community-authored. The textbook problems² include the example from Sec. 2.1. We harvested various query equivalence or query containment benchmarks [1, 2, 4, 5, 48]. Conjunctive SQL and SPARQL queries were manually converted to tableau form.

Figure 3a states the numbers of query pairs by their ground truth w.r.t. QC-CQ (positive/P or negative/N, derived manually). This includes problems that may later be identified as trivial. Figure 3b states the subsets of non-trivial problems that are evaluated in the quantum stage, via annealing (for a polynomial of degree up to 2) and QAOA (for any degree, with maximum occurring degree 4). The former are included in the latter. We state the original number of problems, as well as the reduced number, after simplification.

We designed two synthetic families of *parameterized QC-CQ problems*, based on the directed graph schema \mathbf{S}_g from Example 3.4. Figure 3c illustrates the archetypal building blocks. Family **2-cycle-to- i -chain** contains pairs of a 2-cycle query and a query describing a chain of length i for $i \in \mathbb{N}_{\geq 1}$. For illustration, revisit the queries 2-cycle (q_{2cy}) and 2-chain (q_{2ch}) presented in Example 3.4. Family **2-chain-to- i -star**, contains pairs of a 2-chain query and an i -star query for $i \in \mathbb{N}_{\geq 1}$. All these problems can be solved with annealing and QAOA. They allow for small-stepped scaling in the number of binary variables, which here, map directly to qubits. Moreover, preparation or simplification do not reduce the number of binary variables. (While simplification has no effect, we will enable it by default in our experiments.) The search space is non-trivially exponential, yet we can manually derive two optimal (and only) solutions for each instance as ground truth (details in Appendix D).

Implementation. We implemented the workflow described in Section 4, utilizing Eclipse Qrisp for gate-based QAOA across multiple backends and D-Wave libraries for annealing. Specifically, we use Python 3.10, qrisp 0.7.9, dwave-ocean-sdk 9.0.0, qiskit 2.2.1 and qiskit-aer 0.17.2. To access IQM quantum hardware, we used Python 3.11, qrisp 0.7.17, and qiskit 2.1.2.

¹The probability P^* of obtaining at least one solution grows exponentially with the number of measurements. For example, with a solution probability of only 10% and 20 measurements, the probability for a true positive reaches $P^* = 1 - 0.9^{20} \approx 87.8\%$.

²From (1) “Foundations of Databases” by Abiteboul, Hull, and Vianu [7], (2) the online textbook “Database Theory” by Arenas, Barceló, Libkin, Martens, and Pieris [9] (version from 2022-08-19), (3) the booklet “Answering Queries using Views” by Afrati, Chirkova, and Jagadish [8], (4) lecture material by Koch taught at Saarland University in 2006 (shared in personal communication), and (5) lecture material by Schweikardt [42].

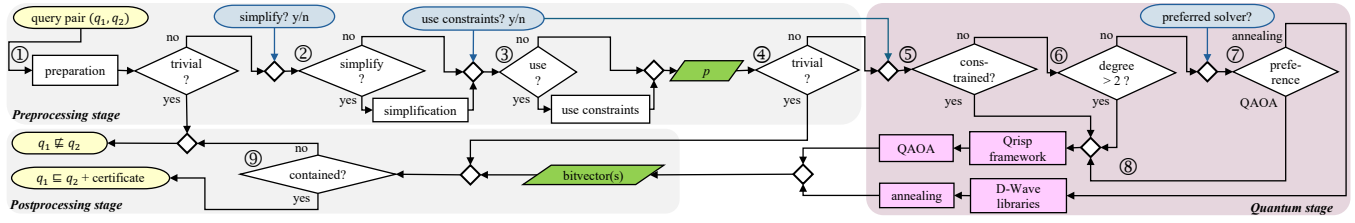


Figure 2: 3-stage workflow: Input problem and output (yellow ovals), parameters (blue ovals), and the decisions leading to evaluation using QAOA or annealing (pink boxes). The polynomial (p) and bitvectors are central artifacts (green parallelograms).

Total	Collection	Anneal.		QAOA	
P N		P	N	P	N
108 81	Original T&B	74	22	87	26
	Simplified T&B	26	2	32	3

2-cycle

2-chain

5-star

(a) T&B (b) Non-trivial T&B (c) Graphs

Figure 3: (a) Query pairs from textbooks and benchmarks, (b) non-trivial subsets, and (c) generic graph building blocks.

Backends. We first describe the *simulators*. For annealing, we use the classical simulated annealer software `SimulatedAnnealingSampler`. The `PathIntegralAnnealingSampler` emulates the behavior of a quantum annealer. To simulate quantum circuit experiments, we use IBM Qiskit’s CPU-based `Aer`. We use four *quantum hardware devices*. For quantum annealing, we use D-Wave’s Advantage System 6.4 and Advantage2 System 1.7. For QAOA, we use IQM Emerald and IBM Aachen. Table 1 provides details on all solvers.

Table 1: Simulators (SW) with their software libraries and quantum hardware devices (HW) with number of qubits.

Abbrev/	Description	Library/Device	Qubits
SA	Sim. annealer	SW dwave-neal 0.6.0	
SQA	Sim. quantum annealer	SW dwave-samplers 1.6.0	
QA-adv	D-Wave quantum annealer	HW Advantage System 6.4	5,612
QA-adv2	D-Wave quantum annealer	HW Advantage2 System 1.7	4,592
AerSim	CPU-based simulator	SW qiskit-aer 0.17.2	
IQM-Emerald	Gate-based QPU	HW IQM Emerald	54
IBM-Aachen	Gate-based QPU	HW IBM Aachen	156

Standard configuration. Unless stated otherwise, we use a standard configuration. For easier comparison, we use the same configuration for experiments with simulators and quantum hardware. We deliberately keep the number of measurements low to ensure that successful outcomes cannot be attributed to random chance and to meet the practical limitations of current hardware.

In annealing, we perform 500 reads. For both simulated annealing and simulated quantum annealing, we use a beta range of $[0.5, 10]$ and the (default) geometric beta schedule. For simulated annealing, we use a fixed initial value. For quantum annealing, we use the (default) linear annealing schedule and an annealing time of $30\mu\text{s}$.

For QAOA, we configure 30 iterations, 2 layers, 500 shots, and constraints. To efficiently simulate large instances, we use the matrix product state method. In simulating QAOA, we limit the number of binary variables to 42. All simulations have a 60-minute timeout.

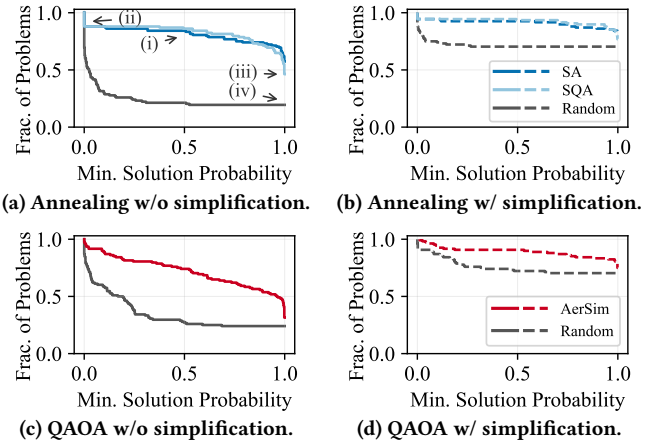


Figure 4: Soundness of 3-stage workflow of positive T&B query pairs (on simulators). Showing fraction of problems where solution probability meets/exceeds a given threshold.

Execution environment. Our experiments run on a Linux server with 2 Intel Xeon Gold 6242R processors (3.1 GHz, 40 cores) and 384 GB RAM. Quantum hardware is accessed as cloud service.

5.3 RQ1: Soundness

We first explore soundness of the entire workflow and then of the quantum stage. We use simulators with standard configuration.

Soundness of end-to-end workflow. We process all positive T&B query pairs from Figure 3a with our 3-stage workflow. This includes problems that are trivial to start with, that become trivial after simplification, and that cannot be solved, as the degree of the polynomial is too high for annealing or where the number of qubits exceeds the simulator capabilities. We measure solution probabilities, and therefore only consider the positive query pairs.

We distinguish two evaluation paths. For the first, we configure annealing as preferred solver and deviate from the workflow in Figure 2: For polynomial degree greater two, we return that the problem instance could not be solved (rather than defaulting to QAOA). For the second, we configure QAOA as preferred solver.

Results. Figure 4 visualizes the results. The plots (a) and (b) show annealing with simplification disabled/enabled. Likewise, the plots (c) and (d) show QAOA with simplification disabled/enabled.

Table 2: Classification outcomes for nontriv. T&B problems.

Collection	Annealing (SA, SQA)					QAOA (AerSim)				
	TP	FP	FN	TN	⊥	TP	FP	FN	TN	⊥
Original T&B	74	/	0	22	0	84	/	0	25	4
Simplified T&B	26	/	0	2	0	32	/	0	3	0

Legend: True/False positives/negatives; ⊥: simulator capacity exceeded.

We plot the fraction of query pairs whose solution probability meets/exceeds a given threshold. That is, for any value on the x -axis, the corresponding value on the y -axis indicates the fraction of pairs that achieved a solution probability greater than or equal to this threshold. To illustrate, we highlight three observations in Figure 4a. Arrow (i) points out that a solution probability of 50% and greater is obtained with simulated annealing for about 80% of the query pairs (which accounts for almost all QUBO instances).

A vertical function block denotes the fraction of problems that have this exact solution probability. Specifically, the leftmost vertical function block (indicated by Arrow (ii) at $x = 0$) shows the fraction of query pairs that could not be solved by our workflow (e.g., too many qubits, or polynomial degree too high for annealing).

The y -value at which the curve ends (see Arrow (iii) at $x = 1$) shows the share of problem instances solved with close to 100% solution probability. For reference, we plot the likelihood of solving the problem by chance (“random”), obtained by generating 500 bitvectors at random. For QAOA, we generate bitvectors that are *valid*: Each represents a matrix with one bit per row set to 1, to be comparable with constrained QAOA where this is enforced.

This likelihood is considerably lower than the measured probabilities (apart from the corner cases of solution probabilities close to zero or one). The y -value at which the random curve ends (Arrow (iv) at $x = 1$) shows the fraction of problems that are trivial. Thus, the difference in fraction between Arrows (iii) and (iv) is the gain that can be contributed to our approach.

Throughout, we observe even higher solution probabilities when simplification is enabled (even for guessing at random).

Discussion. With simplification, more input problems become trivial to start with, and many problems become easier to solve, since the number of binary variables can often be reduced. Our results show that the simplification step is indeed very effective.

In general, problems with high solution probabilities are easy to solve for our approach. It is plausible that we observe many such cases, given that the textbook problems were designed as pencil-and-paper exercises. Even for problems with very low solution probabilities, a single solution found is sufficient to solve a QC-CQ problem. Overall, this **confirms that our workflow can correctly solve nearly all input problems**, esp. with simplification enabled.

Soundness of quantum stage. We now focus on the quantum stage in isolation and only consider the nontrivial T&B problems (Figure 3b). We deliberately include the negative query pairs to check whether our objective function is implemented correctly.

Results. Table 2 reports perfect true positive (TP) and true negative (TN) rates for all T&B problems that the simulators can process (in a small number of QAOA experiments, the number of qubits exceeded the capacities of the simulator, denoted “⊥”). Recall that by design, false positives (FP) cannot occur (denoted “/”). In the experiment shown, we did not observe any false negatives (FN).

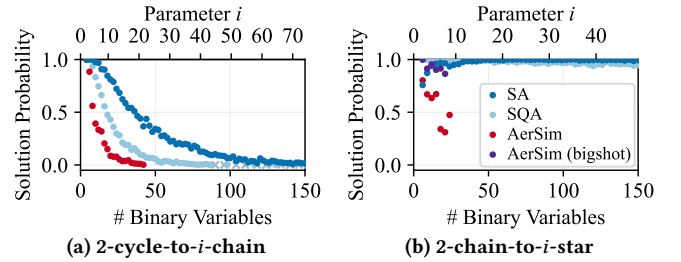


Figure 5: Problem size vs. solution probability for parameterized QC-CQ problems. Scaling behavior is problem-specific.

With annealing, both simulated annealing and simulated quantum annealing (SA and SQA) produce identical results.

We found our experiments to be highly repeatable, with one exception, as QAOA sometimes produces a single false negative.

Discussion. The classification outcomes **confirm the soundness of our implementation for the quantum stage**.

5.4 RQ2: Scalability

Using the parameterized QC-CQ problems, we explore how the probability of solving QC-CQ problems scales with problem size. We use the same setup as before. In addition, we run AerSim with 4 Layers, 100 iterations, and 5,000 shots (referred to as “bigshot”).

Results. Figure 5 shows how the solution probability changes as the size of the input problem increases. The bottom horizontal axis states the number of binary variables in the polynomial, which directly maps to the number of qubits; the top axis states the parameter controlling the problem size. Grey crosses indicate a solution probability of zero (crosses sampled to avoid overplotting).

The scaling behavior for 2-cycle-to- i -chain (Figure 5a) is as expected, and both annealing and QAOA show the same trend: the solution probability decreases as the problem size grows. Simulated annealing reaches larger problem instances, due to the more favorable scaling behavior of the simulator (SA).

However, 2-chain-to- i -star (Figure 5b) displays a strikingly different scaling behavior, and much higher solution probabilities. With simulated annealing (SA), smaller instances even yield lower solution probabilities than larger ones, and the curve quickly reaches 100%, i.e., each read returns an optimal solution. With QAOA (AerSim), the solution probabilities remain higher compared to 2-cycle-to- i -chain, but there is a steep drop until all simulations exceed the timeout. To investigate, we compare with the “bigshot” configuration (purple dots in Figure 5b). Evidently, increasing the number of layers, shots, and iterations improves the solution probabilities.

Discussion. 2-cycle-to- i -chain scales as expected: the solution probability decreases with increasing problem size: Each additional variable increases the probability that the respective heuristic algorithm does not terminate in a global minimum. With QAOA, we exceed the capacity of the simulator sooner.

To better understand the outstanding performance of 2-chain-to- i -star, we investigated the characteristics of this problem family. Section 6 discusses the problem-specific energy landscape, where each local minimum is at the same time a global minimum. This

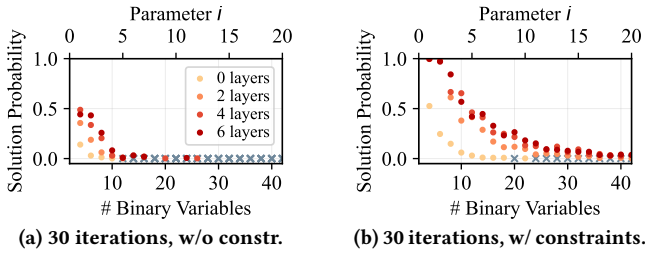


Figure 6: Solution probabilities for 2-cycle-to- i -chain, varying input size and QAOA parameters in simulation (AerSim). The constrained variants (shown right) are always superior.

provides favorable conditions for all solvers. Section 6 also elaborates our hypothesis on what causes slightly inferior performance for small values of the parameter i with simulated annealing (SA).

For QAOA, we observe a clear drop in performance in Figure 5b, yet the solution probabilities are nevertheless higher than in Figure 5a. Our “bigshot” experiment indicates that improving the configuration parameters also improves QAOA performance.

Clearly, the **scaling behavior is problem-specific**. 2-cycle-to- i -chain scales as can be expected based on state-of-the-art, and chain queries of length 20 are no longer small queries. However, **2-cycle-to- i -star surprises with exceptionally good performance**. This strongly motivates further research to investigate QC-CQ problems in terms of their energy landscapes.

5.5 RQ3: Parameter Sensitivity for QAOA

We explore the parameter sensitivity of QAOA on the 2-cycle-to- i -chain family, given its generic scaling behavior. Again, the experiments are run on simulators. We vary the number of layers (0, 2, 4, and 6) and compare the unconstrained and the constrained variant.

Results. Figure 6 shows how the solution probability changes with the input size as we vary QAOA parameters. Again, gray crosses indicate a solution probability of zero. The QC-CQ problem is rarely solved beyond 20 binary variables with zero layers; adding layers lifts the probability. Enabling constraints is very effective.

Discussion. The results confirm that our standard configuration (30 iterations, 2 layers, 500 shots) is reasonable. **QAOA with constraints is very effective** in reducing the solution space and thus increasing the solution probabilities. There are scenarios where we still find solutions for more than 40 binary variables, which is impressive given the exponential search space.

5.6 RQ4: Experiments on Quantum Hardware

We explore how the effects observed with simulators transfer to current quantum hardware. The experiments are run on the four quantum hardware devices using the standard configuration.

Results. Figure 7 shows how the solution probabilities scale for the 2-cycle-to- i -chain problem. As expected, the QC-CQ problems that we can solve on real hardware are much smaller-scale.

With quantum annealing (Figure 7a), we can solve larger problem instances than with QAOA, yet we are limited to QUBO problems. Here, the more recent generation of hardware (D-Wave Advantage2) outperforms the earlier generation (D-Wave Advantage).

Figures 7b³ and 7c show QAOA experiments on devices by IQM and IBM. As in the simulation, the constrained variant outperforms the unconstrained variant. A key difference concerns the effect of increasing the number of layers. Different from the simulator, more layers do not always improve the solution probability.

Discussion. We can **successfully solve QC-CQ problems on real quantum hardware, albeit of smaller size**. Our QAOA experiments on hardware confirm that the **constrained variant is superior**. On an idealized simulator, adding layers increases expressivity and can improve solution probability. Yet on real devices, deeper circuits can accumulate more gate and decoherence errors, which may cause a loss in fidelity.

6 Investigation of Energy Landscapes

To better understand the different scaling behavior of the two parameterized QC-CQ problems (cf. Figure 5), we investigated their energy landscapes (cf. Sec. 2.2). Recall that we aim to minimize the polynomial $p(\bar{x})$ that represents the given query pair (q_1, q_2) . The *energy landscape* of $p(\bar{x})$ refers to the distribution of polynomial values across all possible input bitvectors (in this context called *states*), where (values of) neighboring bitvectors (i.e., they differ in one bit) are considered to be directly connected.

While the two problem families seem similar at first, the energy landscape of 2-chain-to- i -star exhibits two distinguishing structural characteristics. First, it is shaped such that every local minimum is also a global minimum, whereas 2-cycle-to- i -chain exhibits an increasing number of local but not global minima. Therefore, the optimum is much more likely to be reached for the former, as the solvers do not “get stuck” locally. Second, the energy landscape of 2-chain-to- i -star has a large plateau of zero-energy states that is directly connected to all negatively valued (and in particular, the optimal-valued) states. Due to these connections, the optimal value can be found more frequently, which explains the high solution probabilities in Figure 5b. For simulated annealing, however, the direct connections can cause the solver to reversely jump out of the optimum and then “get lost” in the zero-plateau. The probability for that jump decreases with growing i due to larger energy differences. Moreover, the likelihood of “getting lost” in the zero-plateau also decreases, as the relative size of the zero-plateau decreases with growing i . Regarding Figure 5b, we believe that for small i , the simulated annealer sometimes escapes into the zero-plateau, leading to the lower solution probabilities observed on smaller instances. This effect is specific to SA and not observed for (S)QA or QAOA. Appendix E provides further details.

7 Discussion

We discuss our insights along the three stages of our workflow.

Preprocessing. Our experiments show that simplification can be highly effective. Of the query pairs from textbooks and benchmarks, a large share becomes trivial or is reduced to quadratic form, so that they can be directly executed on quantum annealers. This has practical relevance, as it provides access to thousands of qubits, currently a magnitude more than gate-based quantum computers.

³The left plot in Figure 7b is missing a single data point (for 8 binary variables and 3 layers), due to a vendor-side timeout when connecting to the remote device.

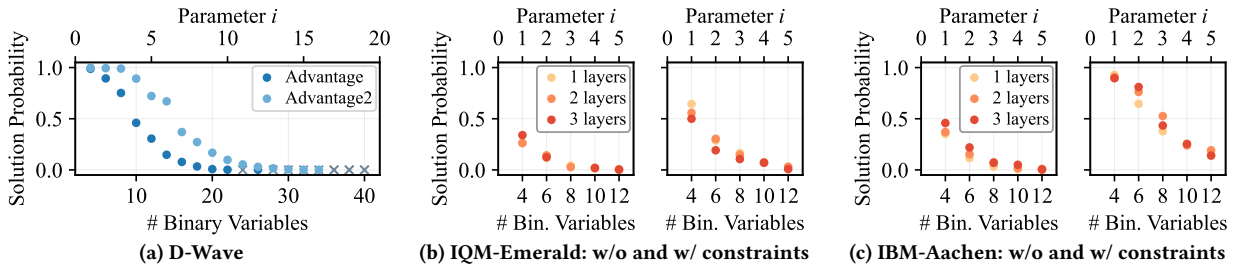


Figure 7: Quantum devices: 2-cycle-to- i -chain on (a) quantum annealers and (b+c) QAOA on gate-based QPUs.

Quantum stage. Our experiments confirm that our approach is sound. We did not custom-tailor the QC-CQ problems to the low-level specifics of the quantum hardware (e.g., QPU topology), as often done in academic explorations. Rather, we included community-authored problem instances, which underlines our success.

We investigated the scaling behavior of two families of parameterized QC-CQ problems. While one exhibits the expected behavior, the other displays consistently high solution probabilities. Our analysis suggests that this can be attributed to the underlying energy landscapes. Exploring the relationship between problem formulation and energy landscape may provide a new research perspective.

We evaluated our algorithm on current quantum hardware. Results across heterogeneous backends suggest generalizability and portability. Despite current hardware limitations, we successfully solved QC-CQ problems at smaller scale. Looking ahead, the gap between simulators and hardware may narrow as vendors improve calibration, reduce error rates, and increase qubit counts.

Postprocessing. Our problem formulation ensures the absence of false positives, and postprocessing produces verifiable witnesses for positive answers. We did not observe high rates of false negatives, which constitute missed opportunities in a database query engine using containment checks for query optimization. These are crucial prerequisites for a future database system integration.

Outlook. We explore a basic three-stage workflow. An orthogonal line of research considers hybrid solvers that combine classical and quantum methods, with QAOA as one component. We also plan to investigate whether auxiliary variables allow reformulating all QC-CQ problems into quadratic form for execution on annealers.

8 Related Work

Query containment is a fundamental decision problem with numerous practical applications. For conjunctive queries under set semantics (the focus here), containment is known to be NP-complete [13]. Under bag semantics, multiplicities matter and the problem becomes substantially more intricate. A characterization analogous to Theorem 2.5 is not known, and it remains open whether the query containment problem is decidable. Recent advances in database theory have established decidability for restricted fragments and undecidability for more expressive query languages, cf. [28, 33].

The problem of deciding *query equivalence* is related. Recent work on equivalence of restricted SQL queries encodes the problem for constraint solvers [15]. In the case of inequivalence, *Cosette* [14] produces a data instance serving as a counterexample. This validates the decision, similarly to the certifying witnesses in our approach.

A line of research has been investigating *quantum computing for cost-based query optimization* [17, 19, 30, 30, 36, 39, 44, 45]. Like most of these works, we also utilize QUBO and QAOA formulations, yet we target semantic query optimization for the first time.

There is a recent trend showing that formulations of database problems originally designed for quantum computing can perform remarkably well when executed on classical hardware. These *quantum-inspired approaches* [40, 41] demonstrate that reformulating classical problems can unlock new solution strategies. Inversely to applying quantum computing to database problems, there are also proposals to apply database theory research to solve quantum computing problems, such as simulating quantum circuits [20, 21].

Within the *quantum algorithms* community, there is an active line of research on quantum formulations for graph structured problems. This includes graph isomorphism [12, 23, 34], which can be seen as a restricted form of graph homomorphism, as well as quantum notions of homomorphisms [32]. While this work is related, the modeling assumptions differ. In quantum algorithms literature, graphs are typically represented by adjacency matrices, while we consider homomorphisms that arise from tableau queries. Thus, existing formulations would require substantial modification.

9 Conclusion

We present a constructive method for discovering a homomorphism that certifies query containment for conjunctive queries under set semantics. Our approach guarantees the absence of false positives and, for the first time, enables experimental evaluation on quantum hardware. Although current quantum devices are not yet suitable for real-world deployment, our results provide a proof of concept that query containment can be translated into an optimization problem and solved on quantum devices, taking a first step toward quantum-powered semantic query optimization.

Acknowledgments

Luisa Gerlach’s contribution was funded by the Deutsche Forschungsgemeinschaft (DFG, German Research Foundation) – Project ID 414984028 – CRC 1404 FONDA (<https://fonda.hu-berlin.de>).

We are grateful to D-Wave’s Leap Quantum LaunchPad program.

We acknowledge the use of IBM Quantum Credits for this work. The views expressed are those of the authors, and do not reflect the official policy or position of IBM or the IBM Quantum team.

References

- [1] 2025. IDNI TML. <https://github.com/IDNI/TML> original-date: 2023-04-26, commit hash f7891ee.
- [2] 2025. Jena SPARQL API. <https://github.com/Scaseco/jena-sparql-api> original-date: 2021-06-21, commit hash 6138a2e.
- [3] 2025. Quantum error correction below the surface code threshold. *Nature* 638, 8052 (2025), 920–926.
- [4] 2025. SPARQL Query Containment Benchmark. <http://sparql-qc-bench.inrialpes.fr/>
- [5] 2025. uwdb/Cosette. <https://github.com/uwdb/Cosette> original-date: 2016-07-21T03:45:45Z, commit hash 7a951aa.
- [6] 2026. D-Wave library. https://docs.dwavequantum.com/en/latest/ocean/api_ref_samplers Visited: 23rd Feb. 2026.
- [7] Serge Abiteboul, Richard Hull, and Victor Vianu. 1995. *Foundations of Databases*. Addison-Wesley. <http://webdam.inria.fr/Alice/>
- [8] Foto Afrati, Rada Chirkova, and H. V. Jagadish. 2019. *Answering Queries Using Views* (2nd ed.). Morgan & Claypool Publishers.
- [9] Marcelo Arenas, Pablo Barceló, Leonid Libkin, Wim Martens, and Andreas Pieris. 2022. *Database Theory*. Open source at <https://github.com/pdm-book/community>. (version from 2022-08-19, visited 2025-10-23).
- [10] Andreas Bärtzsch and Stephan Eidenbenz. 2020. Grover mixers for QAOA: Shifting complexity from mixer design to state preparation. In *2020 IEEE International Conference on Quantum Computing and Engineering (QCE)*. 72–82.
- [11] Umut Çalikylmaz, Sven Groppe, Jinghua Groppe, Tobias Winker, Stefan Prestel, Farida Shagieva, Daanish Arya, Florian Preis, and Le Gruenwald. 2023. Opportunities for Quantum Acceleration of Databases: Optimization of Queries and Transaction Schedules. *Proc. VLDB Endow.* 16, 9 (2023), 2344–2353. doi:10.14778/3598581.3598603
- [12] Cristian S. Calude, Michael J. Dinneen, and Richard Hua. 2017. QUBO formulations for the graph isomorphism problem and related problems. *Theoretical Computer Science* 701 (2017), 54–69. doi:10.1016/j.tcs.2017.04.016 At the intersection of computer science with biology, chemistry and physics - In Memory of Solomon Marcus.
- [13] Ashok K. Chandra and Philip M. Merlin. 1977. Optimal Implementation of Conjunctive Queries in Relational Data Bases. In *Proceedings of the 9th Annual ACM Symposium on Theory of Computing (STOC'77)*. 77–90. doi:10.1145/800105.803397
- [14] Shumo Chu, Daniel Li, Chenglong Wang, Alvin Cheung, and Dan Suciu. 2017. Demonstration of the Cosette Automated SQL Prover. In *Proceedings of the 2017 ACM International Conference on Management of Data, SIGMOD Conference 2017*. 1591–1594. doi:10.1145/3035918.3058728
- [15] Shumo Chu, Brendan Murphy, Jared Roesch, Alvin Cheung, and Dan Suciu. 2018. Axiomatic foundations and algorithms for deciding semantic equivalences of SQL queries. *Proc. VLDB Endow.* 11, 11 (July 2018), 1482–1495. doi:10.14778/3236187.3236200
- [16] Elizabeth Crosson and Aram W Harrow. 2016. Simulated quantum annealing can be exponentially faster than classical simulated annealing. In *2016 IEEE 57th Annual Symposium on Foundations of Computer Science (FOCS)*. 714–723.
- [17] Tobias Fankhauser, Marc E. Soler, Rudolf Marcel Fuchsli, and Kurt Stockinger. 2023. Multiple Query Optimization Using a Gate-Based Quantum Computer. *IEEE Access* 11 (2023), 114031–114043. doi:10.1109/ACCESS.2023.3324253
- [18] Edward Farhi, Jeffrey Goldstone, and Sam Gutmann. 2014. A Quantum Approximate Optimization Algorithm. arXiv:1411.4028 [quant-ph] <http://arxiv.org/abs/1411.4028>
- [19] Maja Franz, Tobias Winker, Sven Groppe, and Wolfgang Mauerer. 2024. Hype or Heuristic? Quantum Reinforcement Learning for Join Order Optimisation. In *IEEE International Conference on Quantum Computing and Engineering, QCE 2024*, Marek Osinski, Brian La Cour, and Lia Yeh (Eds.). 409–420. doi:10.1109/QCE60285.2024.00055
- [20] Floris Geerts and Rihan Hai. 2025. QC meet CQ: Quantum Conjunctive Queries. In *Proceedings of the 2nd Workshop on Quantum Computing and Quantum-Inspired Technology for Data-Intensive Systems and Applications (Q-Data '25)*. 25. doi:10.1145/3736393.3736696
- [21] Rihan Hai, Shih-Han Hung, Tim Coopmans, Tim Littau, and Floris Geerts. 2025. Quantum Data Management in the NISQ Era. *Proc. VLDB Endow.* 18, 6 (2025), 1720–1729. doi:10.14778/3725688.3725701
- [22] Rihan Hai, Shih-Han Hung, and Sebastian Feld. 2024. Quantum Data Management: From Theory to Opportunities. In *40th IEEE International Conference on Data Engineering, ICDE 2024*. 5376–5381. doi:10.1109/ICDE60146.2024.00410
- [23] Richard Hua and Michael J. Dinneen. 2020. Improved QUBO Formulation of the Graph Isomorphism Problem. *SN Comput. Sci.* 1, 1 (2020), 19:1–19:18. doi:10.1007/S42979-019-0020-1
- [24] IBM. 2025. IBM Quantum. <https://quantum.ibm.com/?src=ibm-quantum-homepage> Accessed: 2025-04-01.
- [25] IQM. 2025. IQM Resonance. <https://resonance.meetiqm.com> Accessed: 2025-04-01.
- [26] Ali Javadi-Abhari, Matthew Treinish, Kevin Krsulich, Christopher J. Wood, et al. 2024. Quantum computing with Qiskit. arXiv:2405.08810 [quant-ph] doi:10.48550/arXiv.2405.08810
- [27] Tanuj Khattar and Craig Gidney. 2025. Rise of conditionally clean ancillae for efficient quantum circuit constructions. *Quantum* 9 (May 2025), 1752. doi:10.22331/q-2025-05-21-1752
- [28] George Konstantinidis and Fabio Mogavero. 2019. Attacking Diophantus: Solving a Special Case of Bag Containment. In *Proceedings of the 38th ACM SIGMOD-SIGACT-SIGAI Symposium on Principles of Database Systems, PODS 2019, Amsterdam, The Netherlands, June 30 - July 5, 2019*. ACM, 399–413. doi:10.1145/3294052.3319689
- [29] Hanwen Liu, Abhishek Kumar, Federico M. Spedalieri, and Ibrahim Sabek. 2025. Hybrid Quantum-Classical Optimization for Bushy Join Trees. In *Proceedings of the 2nd Workshop on Quantum Computing and Quantum-Inspired Technology for Data-Intensive Systems and Applications, Q-Data 2025*. 20–24. doi:10.1145/3736393.3736695
- [30] Hanwen Liu, Federico M. Spedalieri, and Ibrahim Sabek. 2025. A Demonstration of Q2O: Quantum-augmented Query Optimizer. *Proc. VLDB Endow.* 18, 12 (2025), 5439–5443. doi:10.14778/3750601.3750691
- [31] David Maier. 1983. *The Theory of Relational Databases*. Computer Science Press. <http://web.cecs.pdx.edu/%7Emaier/TheoryBook/TRD.html>
- [32] Laura Mancinska and David E. Roberson. 2016. Quantum homomorphisms. *J. Comb. Theory B* 118 (2016), 228–267. doi:10.1016/j.jctb.2015.12.009
- [33] Jerzy Marcinkowski and Piotr Ostropolski-Nalewaja. 2025. Bag Semantics Query Containment: The CQ vs. UCQ Case and Other Stories. *Proc. ACM Manag. Data* 3, 5 (2025), 275:1–275:24. doi:10.1145/3767711
- [34] Nicola Mariella and Andrea Simonetto. 2023. A Quantum Algorithm for the Sub-graph Isomorphism Problem. *ACM Transactions on Quantum Computing* 4, 2, Article 13 (Feb. 2023), 34 pages. doi:10.1145/3569095
- [35] Catherine C McGeoch. 2022. *Adiabatic quantum computation and quantum annealing: Theory and practice*. Springer Nature.
- [36] Nitin Nayak, Jan Rehfeld, Tobias Winker, Benjamin Warnke, Umut Çalikylmaz, and Sven Groppe. 2023. Constructing Optimal Bushy Join Trees by Solving QUBO Problems on Quantum Hardware and Simulators. In *Proceedings of the International Workshop on Big Data in Emergent Distributed Environments (BiDEDE '23)*. Article 7, 7 pages. doi:10.1145/3579142.3594298
- [37] Harald Putterman, Kyungjoo Noh, Connor T Hann, Gregory S MacCabe, Shahriar Aghaeimebodi, Rishi N Patel, Menyung Lee, William M Jones, Hesam Moradinejad, Roberto Rodriguez, et al. 2025. Hardware-efficient quantum error correction via concatenated bosonic qubits. *Nature* 638, 8052 (2025), 927–934.
- [38] Atanu Rajak, Sei Suzuki, Amit Dutta, and Bikas K Chakrabarti. 2023. Quantum annealing: An overview. *Philosophical Transactions of the Royal Society A* 381, 2241 (2023), 20210417.
- [39] Manuel Schönberger, Stefanie Scherzinger, and Wolfgang Mauerer. 2023. Ready to Leap (by Co-Design)? Join Order Optimisation on Quantum Hardware. *Proc. ACM Manag. Data* 1, 1 (2023), 92:1–92:27. doi:10.1145/3588946
- [40] Manuel Schönberger, Immanuel Trummer, and Wolfgang Mauerer. 2023. Quantum-Inspired Digital Annealing for Join Ordering. *Proc. VLDB Endow.* 17, 3 (2023), 511–524. doi:10.14778/3632093.3632112
- [41] Manuel Schönberger, Immanuel Trummer, and Wolfgang Mauerer. 2025. Large-Scale Multiple Query Optimisation with Incremental Quantum-Inspired Annealing. *Proc. ACM Manag. Data* 3, 4 (2025), 253:1–253:25. doi:10.1145/3749171
- [42] Nicole Schweikardt. 2023. Lecture Notes on "Database Theory". <https://www2.informatik.hu-berlin.de/logik/lehre/WS23-24/DBTheorie/downloads/DBT-Skript.pdf>
- [43] Raphael Seidel, Sebastian Bock, René Zander, Matic Petrič, Niklas Steinmann, Nikolay Tcholtchev, and Manfred Hauswirth. 2024. Qrisp: A framework for compilable high-level programming of gate-based quantum computers. *arXiv preprint arXiv:2406.14792* (2024).
- [44] Immanuel Trummer. 2025. Cost-Based Query Optimization for Quantum Computation. In *Proceedings of the 2nd Workshop on Quantum Computing and Quantum-Inspired Technology for Data-Intensive Systems and Applications (Q-Data '25)*. 1–2. doi:10.1145/3736393.3736690
- [45] Immanuel Trummer and Christoph Koch. 2016. Multiple Query Optimization on the D-Wave 2X Adiabatic Quantum Computer. *Proc. VLDB Endow.* 9, 9 (2016), 648–659. doi:10.14778/2947618.2947621
- [46] Guifrè Vidal. 2003. Efficient classical simulation of slightly entangled quantum computations. *Physical review letters* 91, 14 (2003), 147902.
- [47] Tobias Winker, Sven Groppe, Valter Uotila, Zhengtong Yan, Jiaheng Lu, Maja Franz, and Wolfgang Mauerer. 2023. Quantum Machine Learning: Foundation, New Techniques, and Opportunities for Database Research. In *Companion of the 2023 International Conference on Management of Data, SIGMOD/PODS 2023*. 45–52. doi:10.1145/3555041.3589404
- [48] Melisachew Wudage Chekol, Jérôme Euzenat, Pierre Genevès, and Nabil Layaida. 2013. Evaluating and Benchmarking SPARQL Query Containment Solvers. In *The Semantic Web - ISWC 2013*. 408–423.
- [49] Gongsheng Yuan, Yuxing Chen, Jiaheng Lu, Sai Wu, Zhiwei Ye, Ling Qian, and Gang Chen. 2024. Quantum Computing for Databases: Overview and Challenges.

- arXiv:2405.12511 [cs.DB] <https://arxiv.org/abs/2405.12511>
- [50] Gongsheng Yuan, Jiaheng Lu, Yuxing Chen, Sai Wu, Chang Yao, Zhengtong Yan, Tuodu Li, and Gang Chen. 2023. Quantum Computing for Databases: A Short Survey and Vision. In *Joint Proceedings of Workshops at the 49th International Conference on Very Large Data Bases (VLDB 2023) (CEUR Workshop Proceedings, Vol. 3462)*. CEUR-WS.org. <https://ceur-ws.org/Vol-3462/QDSM6.pdf>
- [51] René Zander and Colin Kai-Uwe Becker. 2025. Benchmarking multipartite entanglement generation with graph states. *Advanced Quantum Technologies* 8, 1 (2025), 2400239.
- [52] René Zander, Raphael Seidel, Matteo Inajetovic, Niklas Steinmann, and Matic Petric. 2024. Solving the Product Breakdown Structure Problem with constrained QAOA. In *Proc. IEEE International Conference on Quantum Computing and Engineering*. 462–463. doi:10.1109/QCE60285.2024.10356

APPENDIX

A Details omitted in Section 2.2

In this section, we provide for the interested reader more details of the solution techniques (quantum algorithms and simulated annealing) mentioned in Section 2.2 and used to solve the discrete optimization problems formulated in Section 3.

Particular focus is put on quantum computing methods for solving optimization problems of the form

$$\bar{x} \in \arg \min_{\bar{x} \in C} p(\bar{x}). \quad (3)$$

Here, $p: \{0, 1\}^n \rightarrow \mathbb{R}$ is the *objective function*; it is a polynomial on n binary variables $\bar{x} = (x_1, \dots, x_n)$ with real-valued coefficients. The *search space* is the set $C \subseteq \{0, 1\}^n$, and the goal is to find a tuple $\bar{x} \in C$ such that the value $p(\bar{x})$ is as small as possible. This optimization problem is called *unconstrained* if $C = \{0, 1\}^n$, and *constrained* if $C \subsetneq \{0, 1\}^n$.

The polynomial p is given by a finite sum of monomials

$$p(\bar{x}) = \sum_{k \in K} m_k(\bar{x}), \quad \text{with } m_k(\bar{x}) = c_k \cdot \prod_{i \in I_k} x_i, \quad (4)$$

where K is a finite set, c_k is a real-valued coefficient and $I_k \subseteq \{1, \dots, n\}$ for every $k \in K$. The degree of such a monomial $m_k(\bar{x})$ is $\deg m_k(\bar{x}) := |I_k|$, and the degree of p is the maximum degree of its monomials. Since each variable x_i can only be assigned the values 0 and 1, every linear term can also be expressed as a quadratic term by replacing a variable x_i by x_i^2 (due to $0 \cdot 0 = 0$ and $1 \cdot 1 = 1$). In particular, if the degree of p is ≤ 2 , this implies that we can assume without loss of generality that *every* monomial of p has degree exactly 2; this setting is known as *Quadratic Unconstrained Binary Optimization* problems (for short: QUBOs). Therefore, such a polynomial can alternatively be represented by a real-valued upper triangular $n \times n$ -matrix Q , representing the objective function

$$p(\bar{x}) := \bar{x}^T Q \bar{x} = \sum_{i \leq j} q_{ij} \cdot x_i \cdot x_j, \quad (5)$$

where q_{ij} is the entry in row i and column j of Q . Quantum annealing can then be used to find

$$\bar{x} \in \arg \min_{\bar{x} \in C} p(\bar{x}). \quad (6)$$

In this work, we utilize the following quantum computing methods to solve the optimization problems:

- Quantum Approximate Optimization Algorithm (QAOA) for gate-based quantum computers
- Simulated annealing and quantum annealing

A.1 QAOA for gate-based quantum computers

The *Quantum Approximate Optimization Algorithm* (QAOA) [18] was developed to find approximate solutions to combinatorial optimization problems. The algorithm has a hybrid quantum-classical structure in which quantum and classical components alternate. During the quantum part, QAOA evaluates the expected value of the objective function with respect to a parameter-dependent quantum state. The classical output of the measurements on the quantum

circuit acts as a feedback which is processed in the classical part of the algorithm to heuristically compute new parameters for the next quantum iteration. The new parameters are computed with the objective of minimizing the expected value of the objective function, thereby increasing the probability of (near-)optimal results, which eventually converges.

The quantum circuit for QAOA is composed of layers: Each layer is defined by a function of the so-called *mixing Hamiltonian* H_m that describes the initial state and the *problem Hamiltonian*

$$H_p = \sum_{\bar{x} \in \{0,1\}^n} p(\bar{x}) |\bar{x}\rangle \langle \bar{x}|$$

that describes the objective function. For simplicity, one can imagine that for advancing layers in the circuit, the quantum state shifts from the initial state (i.e., the ground state – which is the eigenvector associated with the minimum eigenvalue – of the *mixing Hamiltonian*) towards the solution state (i.e., the ground state of the *problem Hamiltonian*).

To be precise, an initial state $|\psi_0\rangle$ is evolved by alternatingly applying the problem-specific operator

$$U_p(\gamma) = e^{-i\gamma H_p}$$

and the mixer operator

$$U_m(\beta) = e^{-i\beta H_m},$$

where i denotes the complex number $\sqrt{-1}$.

For ℓ layers of QAOA one obtains the parameter-dependent quantum state

$$|\psi_\ell(\beta, \gamma)\rangle = U_m(\beta_\ell) U_p(\gamma_\ell) \cdots U_m(\beta_1) U_p(\gamma_1) |\psi_0\rangle$$

for real parameters $\beta = (\beta_1, \dots, \beta_\ell)$ and $\gamma = (\gamma_1, \dots, \gamma_\ell)$. The expectation of an objective function is measured by repeated preparation and sampling from the state $|\psi_\ell(\beta, \gamma)\rangle$. A classical optimizer that aims to minimize the expectation of the objective function is used to determine the updated parameters (β', γ') , and this procedure is repeated until the optimizer converges. The problem solution is found by sampling from the final state $|\psi_\ell(\beta^*, \gamma^*)\rangle$.

In the unconstrained setting, i.e., when searching for $\bar{x} \in \{0, 1\}^n$, the initial state is prepared as uniform superposition

$$|\psi_0\rangle = \frac{1}{2^{n/2}} \sum_{\bar{x} \in \{0,1\}^n} |\bar{x}\rangle,$$

and the mixer operator is implemented by parameterized single-qubit rotations in constant depth. For the polynomial objective function (4) the operator U_p can be written as

$$U_p(\gamma) = \prod_{k \in K} e^{-i\gamma \sum c_k m_k(\bar{x}) |\bar{x}\rangle \langle \bar{x}|}$$

where we use that $\exp(A+B) = \exp(A)\exp(B)$ if A and B commute, i.e., $[A, B] = AB - BA = 0$.

Observe that the monomials satisfy

$$m_k(\bar{x}) = \begin{cases} 1 & \text{if } x_i = 1 \text{ for all } i \in I_k \\ 0 & \text{otherwise.} \end{cases}$$

Therefore, each unitary in the above product acts on the qubits in I_k diagonally as

$$e^{-i\gamma \sum c_k m_k(\bar{x}) |\bar{x}\rangle \langle \bar{x}|} = \begin{bmatrix} 1 & 0 & 0 & 0 & 0 \\ 0 & 1 & 0 & 0 & 0 \\ 0 & 0 & \ddots & 0 & 0 \\ 0 & 0 & 0 & 1 & 0 \\ 0 & 0 & 0 & 0 & e^{-i\gamma c_k} \end{bmatrix}. \quad (7)$$

This is realized by a so-called multi-controlled phase (MCP) gate that applies a phase shift $\exp(-i\gamma c_k)$ to the states where all qubits in I_k are in state $|1\rangle$. In practice, this multi-qubit gate is decomposed into $O(|I_k|)$ single and two-qubit gates requiring a total depth of $O(|I_k|)$ [27]. If the sets I_{k_1} and I_{k_2} for indices $k_1, k_2 \in K$ are disjoint, the gates can be applied simultaneously. Therefore, the depth of the quantum circuit to apply the problem-specific operator depends on the degree and structure of the polynomial p . E.g., for $p(\bar{x}) = \sum_{k=1}^{n-1} x_k x_{k+1}$ the circuit depth would be constant independent of the number of qubits n . Moreover, for a general quadratic polynomial, the circuit depth would be $O(n)$ since the chromatic index of the complete graph on n vertices is upper bounded by n .

In general, if p is a degree $d \leq n/2$ polynomial (in practice, the number of binary variables is usually much higher than the polynomial degree d), then the problem-specific operator is implemented with $O(d \cdot n^d)$ gates and circuit depth: The number of square-free monomials of degree at most d is $\sum_{k=1}^d \binom{n}{k}$ which is in $O(n^d)$ for a fixed $d \leq n/2$, and implementing a degree d monomial requires $O(d)$ gates and circuit depth.

Constrained QAOA. For constrained optimization problems, the set of feasible solutions $C \subseteq \{0, 1\}^n$ is a strict subset of $\{0, 1\}^n$. Strategies for incorporating such constraints into the QAOA circuit have been introduced [10]. The main idea is that only the subset of feasible solutions is explored and the reduced size of the search space improves the optimization results. This is achieved by constructing a procedure that prepares a uniform superposition of all feasible states

$$|\psi_0\rangle = U_C |0\rangle = \frac{1}{\sqrt{|C|}} \sum_{\bar{x} \in C} |\bar{x}\rangle.$$

Thus, the ability to construct an efficient state preparation procedure depends on the constraints of a specific problem.

For the query containment problem, the search space C is the subset of $\{0, 1\}^{n_1 \cdot n_2}$ such that for n_2 groups of n_1 binary variables exactly one out of each group of binary variables assumes the value of 1 and the rest assume the value of 0, i.e.,

$$C = \left\{ \bar{x} \in \{0, 1\}^{n_1 \cdot n_2} \mid \sum_{r=1}^{n_1} x_{n_1 \cdot s + r} = 1 \forall s \in \{0, \dots, n_2 - 1\} \right\}.$$

In terms of a quantum state, this is realized by an n_2 -fold tensor product of so-called W -states of n_1 qubits each:

$$W = \frac{1}{\sqrt{n_1}} (|10 \dots 0\rangle + |010 \dots 0\rangle + \dots + |0 \dots 01\rangle)$$

A suitable state preparation procedure and an appropriate mixer operator ensure that the QAOA circuit leaves the subspace of feasible solutions invariant; they are provided by circuits of depth $O(n_1)$ [52].

Complexity of QAOA. The main complexity parameters of QAOA are the number of *layers* of the circuit, the number of *iterations* of the classical optimizer, and the number of *shots* performed in each iteration:

The *number of layers* refers to the number of steps between the initial state and the solution state, thus defining the granularity of the discretization. A higher number of layers per circuit is associated with an increasing approximation quality, but at the same time, higher circuit depth and more gates increase the difficulty of a reliable execution on noisy intermediate-scale (NISQ) quantum hardware, which is the kind of quantum hardware that is available nowadays. From the discussion in the previous paragraph it follows that for an arbitrary quadratic polynomial $p(\bar{x})$ of n binary variables, the circuits for QAOA with ℓ layers have a favorable scaling of depth $O(\ell \cdot n)$ for both the constrained and unconstrained version. In general, for a degree $d \leq n/2$ polynomial $p(\bar{x})$, the depth scales polynomially in the number of binary variables n as $O(\ell \cdot d \cdot n^d)$. Hence, they can be efficiently executed on a quantum computer. This is, however, not the case when a classical simulator is used to emulate the behavior of a quantum computer: handling quantum states of n qubits requires storing and manipulating 2^n complex amplitudes.

The *number of iterations* refers to the maximum allowed number of classical optimizations. In each iteration, the quantum circuit is optimized classically based on its performance in the previous iteration. If the quantum circuit can no longer be optimized further (based on the chosen classical optimizer) or the maximum number of iterations is reached, the algorithm terminates.

The explanation of the *number of shots* requires a short review of the connection between the quantum and the classical part of the algorithm. The quantum part of the algorithm returns an expected value of the objective function with respect to the state represented by the quantum circuit, which is then fed into the classical part. In order to estimate the expected value of the objective function without knowing the full probability distribution of possible results of the quantum circuit, the circuit is executed a number of times and its results are measured, leading to an estimation of the expected value as the mean of the measured results. The number of shots refers to the number of executions that are performed for this estimation.

Limitations of NISQ hardware. Currently available quantum hardware is referred to as Noisy Intermediate-Scale Quantum (NISQ) hardware. Only a small number of physical qubits (e.g., up to 156 qubits on state-of-the-art IBM devices) are available, and computations are affected by limitations such as short coherence times that allow only shallow circuits to be run and noise leading to gate and readout errors. In particular, generating highly entangled quantum states across multiple qubits – a key resource in quantum computation – remains challenging [51]. To overcome these limitations, quantum error correction, which combines several physical qubits to build a logical qubit, will be required. To date, there have been encouraging demonstrations of this technology [3, 37], yet significant challenges in hardware and software engineering need to be addressed for quantum computing to mature.

At this point, quantum hardware is accessed mainly through cloud-based services such as IBM Quantum Platform [24] or IQM

Resonance [25]. Hybrid algorithms such as QAOA consist of a feedback loop between quantum and classical computation. This translates to repeated round-trips between the local client and the remote quantum backend. For each iteration, quantum circuits are sent to the remote backend and measurement results are transmitted back to the local client. In addition to latency issues, this also results in being re-queued in every iteration. The latter issue has been addressed by IBM with the “Session” execution mode that provides exclusive access to the QPU. Moving forward, a tighter integration between quantum and classical high-performance computing will enable hybrid programs to run seamlessly and efficiently.

Due to the aforementioned restrictions regarding reliability and limited access to quantum hardware, quantum algorithms and applications thereof are mostly studied using simulators that run on classical hardware. Simulators are software tools that aim to emulate quantum computations. In general, the costs of simulating quantum computations on classical computers increase exponentially in the number of qubits: For a system of n qubits the quantum state is represented by a 2^n -dimensional state vector. E.g., for $n = 40$ storing the state vector requires approximately 16 terabytes ($2^{40} \cdot 16$ bytes) of memory. In practice, if quantum states are sparse or factorized, state vector simulators such as the Qrisp simulator [43] can enable efficient simulations of larger systems of qubits. Moreover, matrix product state simulators (e.g., provided by Qiskit Aer [26]) offer an efficient tool for simulating quantum computations that rely only on a restricted amount of entanglement [46].

A.2 Simulated annealing & quantum annealing

After describing QAOA in the previous subsection, we now present the foundations of two further optimization methods that have been used to solve the QUBOs considered in this work. These methods are referred to as *simulated annealing* and *quantum annealing* (see also Section 2.2).

Simulated annealing: The *simulated annealing* method (cf., Algorithm 1) starts at some initial state $\bar{x} \in C$ having the value $c := p(\bar{x})$. From there, it iterates through C to find a minimizer $\bar{x}_{\min} \in C$ or an approximation of \bar{x}_{\min} . In each iteration, a random neighbor \bar{x}_{new} of \bar{x} is chosen (here, “neighbor” means that one bit is flipped). If $c_{\text{new}} := p(\bar{x}_{\text{new}})$ is smaller than c , it is considered as the current solution. Otherwise, a deterioration is accepted if a probability denoted as *AcceptProb* exceeds a randomly chosen value. To compute *AcceptProb*, a parameter T as well as the difference between the old and new value ($c_{\text{new}} - c$) are required:

$$\text{AcceptProb}(T, c_{\text{new}} - c) = \min\left(1, \exp\left(-\frac{c_{\text{new}} - c}{k_b \cdot T}\right)\right). \quad (8)$$

This expression is adapted from statistical physics. It is known as *Boltzmann distribution*, which yields the probability of measuring an energy c_{new} given a reference energy c and a temperature T . k_b is denoted as *Boltzmann constant*. *AcceptProb* implies that accepting \bar{x}_{new} is less likely if T is low and the difference $c_{\text{new}} - c$ is large. It remains to clarify how the parameter T or the “temperature” T is determined. Here, a monotonically decreasing function *coolingSchedule* is used, yielding for each iteration a value of T . There are several ways to decrease the temperature T . In this work, we vary T geometrically between a high starting temperature T_{high}

and a low temperature T_{low} . The algorithm terminates if T reaches the threshold T_{low} or falls below T_{low} . Another termination criterion is that the number of iterations exceeds N_{sweeps} .

Algorithm 1 Pseudo code for the simulated annealing method.

```

1: INPUT: Function  $p$ , initial state  $\bar{x}$ , temperatures  $T_{\text{high}}$  and  $T_{\text{low}}$ 
2: INPUT: Number of sweeps  $N_{\text{sweeps}}$ 
3: OUTPUT: Approximation of  $\bar{x}_{\text{min}}$ 
4:  $iter = 1$ 
5:  $stop = false$ 
6: while ! $stop$  do
7:    $T = coolingSchedule(T_{\text{high}}, T_{\text{low}}, iter)$ 
8:    $\bar{x}_{\text{new}} = neighborOf(\bar{x})$ 
9:    $c_{\text{new}} = p(\bar{x}_{\text{new}})$ 
10:  if  $c_{\text{new}} < c$  then
11:     $\bar{x} = \bar{x}_{\text{new}}, c = c_{\text{new}}$ 
12:  else if  $AcceptProb(T, c_{\text{new}} - c) > random(0, 1)$  then
13:     $\bar{x} = \bar{x}_{\text{new}}, c = c_{\text{new}}$ 
14:  end if
15:   $iter = iter + 1$ 
16:  if  $T \leq T_{\text{low}}$  or  $iter > N_{\text{sweeps}}$  then
17:     $stop = true$ 
18:  end if
19: end while
20:  $\bar{x}_{\text{min}} = \bar{x}$ 
21: return  $x_{\text{min}}$ 

```

Contrary to *simulated annealing*, the *quantum annealing* method is not inspired by laws from statistical physics, but rather by phenomena occurring in quantum mechanics. One of them is the observation that a quantum mechanical state attains another state by quantum fluctuations or tunneling through thin energy barriers. Emulating this behavior using a heuristic optimization method, we assign to each binary component $x_i \in \{0, 1\}$ of a state $\bar{x} = (x_1, \dots, x_n) \in C$ a qubit q_i . This results in a register of n qubits: $R = q_1 \dots q_n$. The quantum state for qubit q_i is denoted by $|\psi_i\rangle$, which is a superposition of the following states: $\{|0\rangle, |1\rangle\}$. The quantum state of R is given by $|\Psi\rangle$. Next, we modify $|\Psi\rangle$ such that the objective function p in (6) can be represented by a quantum state. Therefore, we consider the following Hamiltonian:

$$H_{p,an} = \sum_{i=1}^n h_i \sigma_i^z + \sum_{i<j} J_{ij} \sigma_i^z \sigma_j^z,$$

where σ_i^z is the Pauli-z operator applied to qubit q_i , and h_i and J_{ij} are real numbers. Applying $H_{p,an}$ to $|\Psi\rangle$ yields the following state:

$$H_{p,an} |\Psi\rangle = \left(\sum_{i=1}^n h_i \sigma_i^z + \sum_{i<j} J_{ij} \sigma_i^z \sigma_j^z \right) |\Psi\rangle = E_{p,an} |\Psi\rangle$$

and the corresponding energy:

$$E_{p,an} = \sum_{i=1}^n h_i (-1)^{\psi_i} + \sum_{i<j} J_{ij} (-1)^{\psi_i} (-1)^{\psi_j} = \sum_{i=1}^n h_i s_i + \sum_{i<j} J_{ij} s_i s_j,$$

with $s_i \in \{-1, 1\}$ for $i \in \{1, \dots, n\}$. Using the transformation $s_i = 1 - 2x_i$, we can reformulate $E_{p,an}$ as follows:

$$E_{p,an} = \sum_{i \leq j} q_{ij} x_i x_j + K \quad \text{with} \quad K = \sum_{i < j} J_{ij} + \sum_{i=1}^n h_i \quad \text{and} \quad (9)$$

$$q_{ij} = \begin{cases} 4J_{ij}, & \text{if } i < j, \\ -2h_i - 2 \sum_{k=1}^{i-1} J_{ki} - 2 \sum_{k=i+1}^n J_{ik}, & \text{if } i = j. \end{cases}$$

The parameters q_{ij} are the entries of the matrix Q defining the objective function p in (5). Apparently, this expression is similar to the objective function of the QUBO (6). Thus, computing the energy of a quantum state produced by $H_{p,an}$ yields the minimal cost for a QUBO (6). The quantum annealer transforms an initial quantum state that can be prepared in an easy way by an initial Hamiltonian H_I into a quantum state governed by the problem Hamiltonian $H_{p,an}$. Thereby, the *adiabatic theorem* is considered. The adiabatic theorem states that if we consider the quantum state Q_I in its ground state (energy minimizing state) and if we transfer this state to the final quantum state $Q_{p,an}$ sufficiently slowly, the process will end up in the ground state of $Q_{p,an}$ with high probability [35, Section 2.2.2]. Thus, after high probability measurement, we obtain the ground state and its energy $E_{p,an}$. This is made possible by quantum fluctuations or tunneling through energy barriers in the energy landscape of the final quantum state. Now, the crucial step consists in preparing the state $H_{p,an} |\Psi\rangle$ and measuring its energy. Therefore, we consider an initial state produced by the Hamiltonian

$$H_I = \sum_{i=1}^n \frac{1 - \sigma_i^x}{2},$$

where σ_i^x is the Pauli-x operator for qubit q_i . Applying H_I yields a superposition of the different quantum states in R such that in the ground state of H_I (energy minimizing state) every quantum state in R is equally likely to be observed. Combining H_I and $H_{p,an}$, we obtain a Hamiltonian depending on a variable s parameterized by t :

$$H(s(t)) = A(s(t)) H_I + B(s(t)) H_{p,an}.$$

The function $s : [0, t_f] \rightarrow [0, 1]$ is known as *annealing path* and has to be specified by the user. In this work, we consider a linear function:

$$s(t) = \frac{t}{t_f},$$

where t_f is denoted as *annealing time*. A and B are called *envelope functions*, having the following properties:

$$A(0) \gg B(0) \quad \text{and} \quad A(1) \ll B(1),$$

which means that for $t = 0$ the Hamiltonian is governed by H_I , while at the end of the annealing path for $t = t_f$ the Hamiltonian is governed by $H_{p,an}$. In addition to that, A decreases monotonically in s , while B increases monotonically in s . Thus, as t increases, $H(s(t))$ approaches $H_{p,an}$. Finally, the qubit values $|\psi_i\rangle$ are measured. Using

$$(-1)^{\psi_i} = s_i = 2x_i - 1, \quad (10)$$

a minimizer \bar{x}_{\min} of (6) and a minimal value of p can be determined. The physical interpretation of this method reads as follows: Applying the initial Hamiltonian introduces energy to the annealing process in the form of quantum fluctuations.

Adapting A and B allows us to change between different minima of the energy landscape by tunneling through energy barriers that separate them. If the energy barriers are thin, the probability of tunneling increases. In contrast to simulated annealing, the probability governing the change between local minima is not affected by the difference between the minima. Exploiting the tunneling phenomenon, we can move faster and further across the energy landscape compared to the simulated annealing method, since within a single iteration of the simulated annealing method, one has to “climb” over energy barriers according to the Boltzmann distribution instead of tunneling through the energy barriers. During the annealing process, the energy landscape is more and more adapted to the QUBO considered. If A and B are modified sufficiently slowly, the whole process will finish in an energy minimizing ground state with high probability due to the adiabatic theorem. Since A and B change gradually, this method can be assigned to the class of annealing based optimization methods. The whole method is summarized in Algorithm 2.

Algorithm 2 Pseudo code for the quantum annealing method.

- 1: **INPUT:** Parameters q_{ij} , annealing time t_f
 - 2: **INPUT:** Number of sweeps N_{sweeps}
 - 3: **OUTPUT:** Approximation of \bar{x}_{\min}
 - 4: $iter = 0$, $stop = false$
 - 5: $\Delta t = \frac{t_f}{N_{\text{sweeps}}}$
 - 6: Compute the weights h_i and J_{ij} using (9) to obtain $H_{p,an}$
 - 7: Apply H_I scaled by $A(0)$ to obtain a quantum state $|\Psi\rangle$
 - 8: **for** $iter < N_{\text{sweeps}}$ **do**
 - 9: $t = iter \cdot \Delta t$, $s(t) = \frac{t}{t_f}$
 - 10: Determine $A(s(t))$ and $B(s(t))$
 - 11: Determine $H(s(t))$ and apply it to $|\Psi\rangle$
 - 12: $iter = iter + 1$
 - 13: **end for**
 - 14: Measure $|\Psi\rangle$ to obtain the quantum states Ψ_i of the qubits \mathbf{q}_i
 - 15: Use Equation (10) to compute the binary values x_i
 - 16: $\bar{x}_{\min} = \bar{x} = (x_1, \dots, x_n)$
 - 17: **return** \bar{x}_{\min}
-

B Details omitted in Section 3

The following can be easily verified:

Fact B.1. For all $\bar{x} \in \{0, 1\}^{B_2 \times A_1}$ we have:

- (a) $p_{\text{fct}}(\bar{x}) \in \mathbb{N}$, and
- (b) $p_{\text{fct}}(\bar{x}) = 0 \iff$ for every $i \in B_2$ we have $\sum_{j \in A_1} x_{i,j} \leq 1$ (i.e., there is at most one $j \in A_1$ with $x_{i,j} = 1$).

Clearly, when given an $\bar{x} \in \{0, 1\}^{B_2 \times A_1}$ with $p_{\text{fct}}(\bar{x}) \geq 1$, then \bar{x} does *not* represent any function $h: B_2 \rightarrow A_1$.

PROOF OF LEMMA 3.6.

(a) is obvious. For (b) consider an arbitrary assignment $\bar{x} \in \{0, 1\}^{B_2 \times A_1}$ with $p_{\text{fct}}(\bar{x}) = 0$. From Fact B.1 we know that for every $i \in B_2$ there

is at most one $j \in A_1$ with $x_{i,j} = 1$. Consider the extended bit-matrix $\bar{x}^{(e)}$ associated with \bar{x} .

First of all, for contradiction assume that $p_{R,u}(\bar{x}) \notin \{-1, 0\}$. Then there must exist two distinct tuples $w = (w_1, \dots, w_r)$ and $w' = (w'_1, \dots, w'_r)$ in $\mathbf{T}_1(R)$ such that

$$\prod_{k=1}^r x_{u_k, w_k}^{(e)} = 1 \quad \text{and} \quad \prod_{k=1}^r x_{u_k, w'_k}^{(e)} = 1.$$

Since $w \neq w'$, there is a $k \leq r$ such that $w_k \neq w'_k$. In particular, $x_{u_k, w_k}^{(e)} = 1 = x_{u_k, w'_k}^{(e)}$. By definition of $\bar{x}^{(e)}$ this implies that $u_k \in B_2$ and $x_{u_k, w_k} = 1 = x_{u_k, w'_k}$. But this means that for $i := u_k \in B_2$ there are two distinct values $j := w_k$ and $j' := w'_k$ with $x_{i,j} = 1$ and $x_{i,j'} = 1$, contradicting Fact B.1. This proves that $p_{R,u}(\bar{x}) \in \{-1, 0\}$.

Concerning the second statement of (b), we first prove the direction “ \Leftarrow ”. Let us assume that the condition to the right of the symbol “ \iff ” is satisfied. Then, for every $k \leq r$ we have $x_{u_k, z_k}^{(e)} = 1$ and $x_{u_k, z}^{(e)} = 0$ for all $z \in A_1 \setminus \{z_k\}$. Hence, $\prod_{k=1}^r x_{u_k, z_k}^{(e)} = 1$ and for every $(w_1, \dots, w_r) \in \mathbf{T}_1(R)$ with $(w_1, \dots, w_r) \neq (z_1, \dots, z_r)$ we have $\prod_{k=1}^r x_{u_k, w_k}^{(e)} = 0$. Thus, $p_{R,u}(\bar{x}) = -1$. This completes the proof of the direction “ \Leftarrow ”.

For proving the direction “ \Rightarrow ”, let us assume that $p_{R,u}(\bar{x}) = -1$. Thus, there is a tuple $(z_1, \dots, z_r) \in \mathbf{T}_1(R)$ such that $\prod_{k=1}^r x_{u_k, z_k}^{(e)} = 1$, i.e., $x_{u_k, z_k}^{(e)} = 1$ for every $k \leq r$. All that remains to be done is to show that for every $k \leq r$ we have $\sum_{z \in A_2} x_{u_k, z}^{(e)} = 1$. Consider an arbitrary $k \leq r$. If $u_k \in B_2$ then $x_{u_k, z}^{(e)} = x_{u_k, z}$ for all $z \in A_1$, and hence from $p_{\text{fct}}(\bar{x}) = 0$ and Fact B.1(b) and $x_{u_k, z_k} = 1$ we obtain that $\sum_{z \in A_1} x_{u_k, z}^{(e)} = 1$. On the other hand, if $u_k \in A_2 \setminus B_2$, then by definition of the extended bit-matrix $\bar{x}^{(e)}$ we obtain that $\sum_{z \in A_1} x_{u_k, z}^{(e)} \leq 1$. Combining this with the fact that $x_{u_k, z_k}^{(e)} = 1$ and $z_k \in A_1$ yields $\sum_{z \in A_1} x_{u_k, z}^{(e)} = 1$. This completes the proof of Lemma 3.6. \square

PROOF OF LEMMA 3.8.

(a) immediately follows from Lemma 3.6(a) and the definition of $p_{(3)}(\bar{x})$.

For (b) consider an arbitrary $\bar{x} \in \{0, 1\}^{B_2 \times A_1}$ with $p_{\text{fct}}(\bar{x}) = 0$. From Lemma 3.6(b) we obtain that $p_{R,u}(\bar{x}) \in \{-1, 0\}$ for all $R \in \mathbf{S}$ and $u \in \mathbf{T}_2(R)$. Thus, according to the definition of $p_{(3)}(\bar{x})$ we obtain: $p_{(3)}(\bar{x}) \geq -\sum_{R \in \mathbf{S}} |\mathbf{T}_2(R)| = -|\mathbf{T}_2|$. This proves the first statement of (b).

Concerning the second statement of (b), we first prove the direction “ \Rightarrow ”. By assumption, $p_{(3)}(\bar{x}) = -|\mathbf{T}_2| = -\sum_{R \in \mathbf{S}} |\mathbf{T}_2(R)|$. From the definition of $p_{(3)}(\bar{x})$ and the first statement of Lemma 3.6(b) we obtain that $p_{R,u}(\bar{x}) = -1$ for all $R \in \mathbf{S}$ and all $u \in \mathbf{T}_2(R)$. Applying the second statement of Lemma 3.6(b) to all $R \in \mathbf{S}$ and all $u \in \mathbf{T}_2(R)$, we obtain that for all $i \in \text{vars}(\mathbf{T}_2) \cup \text{cons}(\mathbf{T}_2)$ we have $\sum_{j \in A_1} x_{i,j}^{(e)} = 1$. Note that $A_2 = \text{vars}(\mathbf{T}_2) \cup \text{cons}(\mathbf{T}_2) \cup \text{cons}(v_2)$. Furthermore, since we did not already stop during the preparation step, $\text{cons}(v_2) \subseteq \text{cons}(v_1) \subseteq A_1$, and hence according to the definition of the extended bit-matrix $\bar{x}^{(e)}$ we have $\sum_{j \in A_1} x_{i,j}^{(e)} = 1$ for every $i \in \text{cons}(v_2)$. In summary, this yields that $\bar{x}^{(e)}$ represents the mapping $h: A_2 \rightarrow A_1$ defined for every $i \in A_2$ by letting $h(i) = j_i$ where j_i is the uniquely determined $j \in A_1$ with $x_{i,j}^{(e)} = 1$. By applying the second statement of Lemma 3.6(b) to all $R \in \mathbf{S}$ and all $u \in \mathbf{T}_2(R)$,

we furthermore obtain that $(h(u_1), \dots, h(u_r)) \in \mathbf{T}_1(R)$ for all $R \in \mathbf{S}$ and all $u = (u_1, \dots, u_r) \in \mathbf{T}_2(R)$. This proves that condition (3) of Definition 2.4 is satisfied. As conditions (1) and (2) are satisfied by the definition of $\bar{x}^{(e)}$ and the fact that we did not stop already during the preparation step, the mapping h is a homomorphism from q_2 to q_1 . This completes the proof of the direction “ \implies ”.

Let us now turn to the direction “ \impliedby ”. We assume that the condition to the right of the symbol “ \impliedby ” is satisfied. Then, for every $i \in A_2$ there is a $j_i \in A_1$ with $x_{i,j_i}^{(e)} = 1$ and $x_{i,j}^{(e)} = 0$ for all $j \in A_1 \setminus \{j_i\}$; and the mapping $h: A_2 \rightarrow A_1$ defined via $h(i) = j_i$ for all $i \in A_2$ is a homomorphism from q_2 to q_1 . This implies that for every $R \in \mathbf{S}$ and every $u \in \mathbf{T}_2(R)$ the condition to the right of the symbol “ \impliedby ” of Lemma 3.6(b) is satisfied. Hence, from Lemma 3.6(b) we obtain that $p_{R,u}(\bar{x}) = -1$ for every $R \in \mathbf{S}$ and every $u \in \mathbf{T}_2(R)$. According to the definition of $p_{(3)}(\bar{x})$, we hence obtain that $p_{(3)}(\bar{x}) = \sum_{R \in \mathbf{S}} \sum_{u \in \mathbf{T}_2(R)} -1 = -|\mathbf{T}_2|$. This completes the proof of Lemma 3.8. \square

PROOF OF THEOREM 3.9.

Consider an arbitrary bit-matrix $\bar{x} \in C_{gen}$. From Fact B.1(a) we know that $p_{fct}(\bar{x}) \in \mathbb{N}$. Using Lemma 3.8(a) we obtain that $-|\mathbf{T}_1| \cdot |\mathbf{T}_2| \leq -\sum_{R \in \mathbf{S}} |\mathbf{T}_1(R)| \cdot |\mathbf{T}_2(R)| \leq p_{(3)}(\bar{x}) \leq 0$.

If $p_{fct}(\bar{x}) \geq 1$, then $p_{gen}(\bar{x}) \geq p_{(3)}(\bar{x}) + (|\mathbf{T}_1| \cdot |\mathbf{T}_2| + 1) \geq 1$. If $p_{fct}(\bar{x}) = 0$, then $p_{gen}(\bar{x}) = p_{(3)}(\bar{x})$, and from Lemma 3.8(b) we obtain that $d_{gen} \leq p_{(3)}(\bar{x}) \leq 0$. This, in particular, proves the theorem’s first statement.

Let us now turn to the direction “ \impliedby ” of the theorem’s second statement. I.e., we assume that $q_1 \sqsubseteq q_2$, and our aim is to show that $\min_{\bar{x} \in C_{gen}} p_{gen}(\bar{x}) = d_{gen}$. Above, we have already shown that $\min_{\bar{x} \in C_{gen}} p_{gen}(\bar{x}) \geq d_{gen}$. From Theorem 2.5 and $q_1 \sqsubseteq q_2$ we obtain that there exists a homomorphism h from q_2 to q_1 . Let $\bar{x} \in \{0, 1\}^{B_2 \times A_1} = C_{gen}$ be the bit-matrix associated with the mapping h , and let $\bar{x}^{(e)}$ be the corresponding extended bit-matrix. By definition we have $p_{fct}(\bar{x}) = 0$, and from Lemma 3.8(b) we obtain that $p_{(3)}(\bar{x}) = d_{gen}$. Considering the definition of the polynomial p_{gen} and using the fact that $p_{fct}(\bar{x}) = 0$, we obtain that $p_{gen}(\bar{x}) = p_{(3)}(\bar{x}) = d_{gen}$. This proves that $\min_{\bar{x} \in C_{gen}} p_{gen}(\bar{x}) = d_{gen}$, i.e., it proves the direction “ \impliedby ” of the theorem’s second statement.

Let us now turn to the theorem’s third statement and to the direction “ \implies ” of the theorem’s second statement. We have already proved the theorem’s first statement, and thus $\min_{\bar{x} \in C_{gen}} p_{gen}(\bar{x}) \geq d_{gen}$. Consider an $\bar{x} \in C_{gen}$ with $p_{gen}(\bar{x}) = d_{gen}$. Since $d_{gen} \leq 0$, we know that $p_{fct}(\bar{x}) = 0$ (because otherwise we would have $p_{fct}(\bar{x}) \geq 1$ and $p_{gen}(\bar{x}) \geq 1$). Hence, $p_{gen}(\bar{x}) = p_{(3)}(\bar{x})$. Using that $d_{gen} = -|\mathbf{T}_2|$, we obtain from Lemma 3.8(b) that the extended bit-matrix $\bar{x}^{(e)}$ associated with \bar{x} represents a homomorphism from q_2 to q_1 . From Theorem 2.5 we obtain that $q_1 \sqsubseteq q_2$. This completes the proof of Theorem 3.9. \square

Details on how it can happen that polynomial p does not contain any binary variable:

If the polynomial p actually does not contain any binary variable, then $p(\bar{x})$ is the constant function ℓ , for some integer ℓ (for short: $p(\bar{x}) \equiv \ell$). This happens

- for p_{gen}^c , if for all $R \in \mathbf{S}$, all $u = (u_1, \dots, u_r) \in \mathbf{T}_2(R)$, and all $w = (w_1, \dots, w_r) \in \mathbf{T}_1(R)$ there either is a $k \leq r$ with $u_k \in A_2 \setminus B_2$ and $x_{u_k, w_k}^{(e)} = 0$, or $u_k \in A_2 \setminus B_2$ for all $k \leq r$,
- for p_{sim}^c , if for all $R \in \mathbf{S}$, all $u = (u_1, \dots, u_r) \in \mathbf{T}_2(R)$, and all $w = (w_1, \dots, w_r) \in \mathbf{T}_1(R)$ there either is a $k \leq r$ with $u_k \in A_2 \setminus B_2^{(s)}$ and $x_{u_k, w_k}^{(s)} = 0$, or $u_k \in A_2 \setminus B_2^{(s)}$ for all $k \leq r$,
- for p_{gen} , if $B_2 = \emptyset$, and
- for p_{sim} , if $B_2^{(s)} = \emptyset$.

C Details omitted in Section 4

Figure 8 shows the backends of our system architecture required for the quantum stage in Figure 2. This includes software libraries, simulator software running on classical hardware, as well as quantum hardware accessed as cloud services.

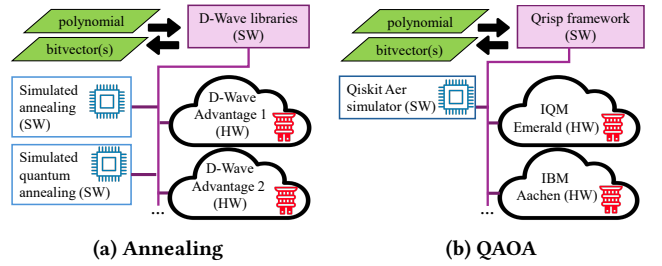


Figure 8: Architecture for (a) annealing and (b) QAOA. Software libraries take polynomials and return bitvectors. Simulators (“SW”/blue icons) run on classical hardware, quantum hardware (“HW”/red icons) accessed as cloud services.

D Details omitted in Section 5.2

Figure 9 visualizes building blocks for our generated query families.

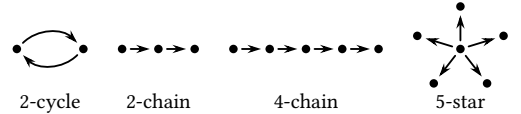


Figure 9: Building blocks for parameterized QC problems.

Both problem families have a configurable parameter i to scale up the problem size by adapting the size of the second query. In particular, we defined the problem families as follows.

Definition D.1 (2-cycle to i -chain). 2-cycle to i -chain is defined as the family of query pairs (q_{2cy}, q_{i-ch}) with q_{2cy} being defined as in Example 3.4 except for renaming the variables from Z, Z' to Z_0, Z_1 , i.e., choosing $\mathbf{T}_{2cy}(E) = \{(Z_0, Z_1), (Z_1, Z_0)\}$ (this change in notation will come in handy later) and $q_{i-ch} := (\mathbf{T}_{i-ch}, v_{i-ch})$ being defined via $v_{i-ch} = ()$ and $\mathbf{T}_{i-ch}(E) = \{(Y_{k-1}, Y_k) : 1 \leq k \leq i\}$, for $i \in \mathbb{N}_{\geq 1}$.

Definition D.2 (2-chain to i -star). 2-chain to i -star is defined as the family of query pairs (q_{2ch}, q_{i-st}) with q_{2ch} being defined as in Example 3.4 and $q_{i-st} := (\mathbf{T}_{i-st}, v_{i-st})$ being defined via $v_{i-st} = ()$ and $\mathbf{T}_{i-st}(E) = \{(Y_0, Y_k) : 1 \leq k \leq i\}$, for $i \in \mathbb{N}_{\geq 1}$.

The number of nodes in the first query determines the stepsize by which we can scale up the number of binary variables. By choosing a query with two nodes (2-cycle) and a query with 3 nodes (2-chain) as the first query, we ensure that they can be scaled up evenly and in small steps, without requiring too many additional binary variables. This is particularly important for experiments on real quantum hardware, which is still very limited in its physical resources.

As mentioned earlier, the queries were carefully crafted to not be simplified in either the preparation or the simplification step. The former is achieved by treating our queries as Boolean queries. Otherwise, for example, fixing the endpoints of the regarded graph queries would lead to trivial query pairs. The latter is achieved by having more than one edge in each first query to avoid any trivial mappings.

For graph queries, certifying the query containment is equivalent to finding a homomorphism between the two represented graphs. In each generated problem instance, two distinct homomorphisms can be found, serving as a ground truth for our examples. In the following, we describe the generation of the ground truth and the problem formula for each family.

2-cycle to i-chain. We can find a homomorphism from an i -chain to a 2-cycle by “wrapping” the chain around the 2-cycle. Depending on where we start this (left or right node of the 2-cycle), we obtain two different possibilities. This provides two distinct homomorphisms that solve the containment problem for every $i \in \mathbb{N}_{\geq 1}$. More formally, the first homomorphism h is given via $h(Y_k) = Z_0$ if k is even and $h(Y_k) = Z_1$ if k is odd (for $0 \leq k \leq i$). The second homomorphism h' is defined the other way round, via $h'(Y_k) = Z_1$ if k is even and $h'(Y_k) = Z_0$ if k is odd (for $0 \leq k \leq i$). Each of these two individual solutions can be specified by the mapping of the first vertex Y_0 of the i -chain to either Z_0 or Z_1 of the 2-cycle, because this uniquely determines the rest of the homomorphism; mapping the other vertices follows accordingly. See Figure 10a for a visualization, where the two mappings are indicated in blue and yellow. Since we can find a homomorphism from the i -chain to the 2-cycle, the latter is contained in the former (but not vice versa). The ground truth is given by these two homomorphisms. Their bit-matrix representations have $i+1$ rows Y_0, \dots, Y_i and 2 columns Z_0, Z_1 ; for any two consecutive rows, one is of the form 10 and the other is of the form 01; and the bit-matrix for h starts with row 10, while the bit-matrix for h' starts with row 01. Each of these two bit-matrices is represented by the bitvector obtained by concatenating the rows of the matrix, i.e., h is represented by the bitvector 10011001 \dots , and h' is represented by the bitvector 01100110 \dots .

However, finding such a homomorphism algorithmically via minimizing the associated polynomial $p(\bar{x})$ is not trivial, since the polynomial contains $2(i+1)$ binary variables ($i+1$ nodes from the i -chain each can be mapped to 2 possible nodes in the 2-cycle), leading to a search space size of $2^{2(i+1)}$ in the unconstrained setting and 2^{i+1} in the constrained setting. Therefore, this problem combines an exponentially large search space (expensive) with small steps of 2 in the number of qubits (scalable). Concerning the resulting problem polynomials, note that

- $p_{(3)}(\bar{x}) = -\sum_{k=1}^i (x_{Y_{k-1}, Z_0} \cdot x_{Y_k, Z_1} + x_{Y_{k-1}, Z_1} \cdot x_{Y_k, Z_0})$,
- $p_{\text{fct}}(\bar{x}) = \sum_{k=0}^i (x_{Y_k, Z_0} \cdot x_{Y_k, Z_1})$,
- $|\mathbf{T}_{2\text{cy}}| \cdot |\mathbf{T}_{i\text{-ch}}| + 1 = 2i+1$, and

thus, the resulting polynomial for *2-cycle to i-chain* has the form:

$$p_{2\text{cy}_i\text{-ch}}(\bar{x}) = p_{(3)}(\bar{x}) + \underbrace{(2i+1) \cdot p_{\text{fct}}(\bar{x})}_{\text{only present in unconstr. setting}}.$$

It can be verified that this polynomial does not get reduced by simplification, and every binary variable actually occurs in the polynomial. Moreover, the polynomial is of degree 2, thus the problem is in QUBO form, which allows to compare annealing and QAOA.

2-chain to i-star. In order to find a homomorphism from an i -star to a 2-chain, a necessary condition is to map the central node of the star to a node with an outgoing edge. There are two possibilities to do so, which lead to two homomorphisms h and h' , given via $h(Y_0) = Z_0$ and $h(Y_k) = Z_1$ or $h'(Y_0) = Z_1$ and $h'(Y_k) = Z_2$ for all k with $1 \leq k \leq i$. The bit-matrix representations of h and h' have $i+1$ rows Y_0, \dots, Y_i and 3 columns Z_0, Z_1, Z_2 . Concerning h , the row for Y_0 is of the form 100, and all further rows are of the form 010. Concerning h' , row Y_0 has the form 010, and all further rows are of the form 001. Concatenating the rows of each bit-matrix yields their bitvector representations 100010010 \dots 010 and 010001001 \dots 001. Importantly, mapping the central node Y_0 already determines the solution. This is illustrated in Figure 10b, where the two mappings are indicated in blue and yellow.

Similarly to the other family, we chose a problem with a small-stepped number of qubits, in this case 3($i+1$), and a reasonably large search space of $2^{3(i+1)}$ solution candidates in the unconstrained setting and 3^{i+1} candidates in the constrained setting. Furthermore, this problem family also leads to polynomials that are of degree 2 and are not affected by simplification. This enables us to perform a thorough scalability analysis and ensures comparability of the two algorithmic approaches.

Concerning the resulting problem polynomials, note that

- $p_{(3)}(\bar{x}) = -\sum_{k=1}^i (x_{Y_0, Z_0} \cdot x_{Y_k, Z_1} + x_{Y_0, Z_1} \cdot x_{Y_k, Z_2})$,
- $p_{\text{fct}}(\bar{x}) = \sum_{k=0}^i (x_{Y_k, Z_0} \cdot x_{Y_k, Z_1} + x_{Y_k, Z_0} \cdot x_{Y_k, Z_2} + x_{Y_k, Z_1} \cdot x_{Y_k, Z_2})$,
- $|\mathbf{T}_{2\text{ch}}| \cdot |\mathbf{T}_{i\text{-st}}| + 1 = 2i+1$, and

thus, the resulting polynomial for *2-chain to i-star* has the form:

$$p_{2\text{ch}_i\text{-st}}(\bar{x}) = p_{(3)}(\bar{x}) + \underbrace{(2i+1) \cdot p_{\text{fct}}(\bar{x})}_{\text{only present in unconstr. setting}}.$$

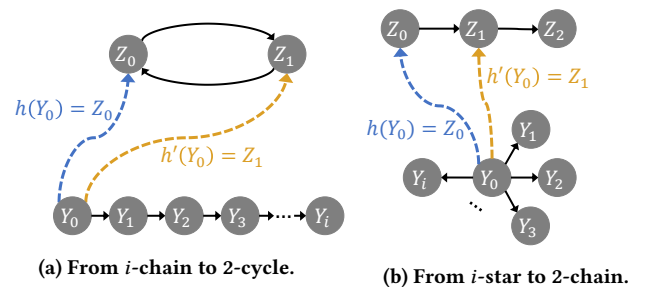


Figure 10: Two distinct homomorphisms, determined by blue/yellow mapping of Y_0 , certify query containment.

E Details omitted in Section 6

The actual performance of the algorithms considered in this paper depends on the individual problem structure. While they have a certain expected performance on average, problem families can be constructed to precisely fit or not fit the nature of the algorithm. Such differences can become more apparent when artificial examples are considered. The course of our algorithms is influenced by the energy landscape that is explored during the run. Recall that we represent a query pair (q_1, q_2) , for which we want to decide whether $q_1 \sqsubseteq q_2$ holds, by a polynomial $p(\bar{x})$. Every possible value of $p(\bar{x})$ for an assignment of the binary variables \bar{x} with 0-1-values, can be regarded as an “energy level” or “value” of the objective function $p(\bar{x})$. Thus, every possible solution candidate (i.e., assignment of \bar{x} with 0-1-values; henceforth they will be called “bitvectors”, “states” or “candidates”) corresponds to a point on the energy landscape.

The overall goal is to reach the global minimum by an annealing-inspired process. As explained in Section 2.2 and Section A.2, the simulated annealing algorithm strives for states of lower or similar energy while sometimes (with exponentially decreasing probability) exploring neighboring states of higher energy than the current one (see the definition of *AcceptProb* in Equation (8) of Section A.2).

As we will see, the experimental results can be explained by differences in the distribution and connectedness of energy levels, so let us take a closer look at the corresponding energy landscapes. We first give an overview of the visible macro-effects and follow with a more detailed computation of the individual relevant sizes.

Overview. Here, we focus on (q_1, q_2) being either the family of query pairs *2-cycle to i-chain* or the family of query pairs *2-chain to i-star*, for $i \in \mathbb{N}_{\geq 1}$. Our goal is to gain a better understanding of the observed scaling behavior depicted in Figure 5. For both families, the energy levels can be partitioned into a very large portion of positive-valued states representing invalid candidates, where at least one row of the represented matrix has more than one bit set to 1 (pos states), a number of zero-valued states representing incorrect mappings with respect to the tuples in q_2 (zero states), and an amount of negative-valued states representing at least partially correct mappings (neg states). The relative size of pos states approaches 100% as i grows, and there is an increasing energy gap of $2i+1$ to the zero and neg states, which is defined by the chosen “penalty weight” $|T_1| \cdot |T_2| + 1$. For the small portion of zero and neg states, it is worth investigating the development of their proportions towards each other. While both families start off with a relatively large zero plateau, its fraction declines towards 0 for *2-cycle to i-chain* and approaches a 50/50 balance with the neg states for *2-chain to i-star*. A summary of the development of all ratios is given in Table 3. In order to interpret these ratios with respect to the experimental results, we also need to investigate the connectedness of the states.

Figure 11 illustrates the connectedness of the energy landscapes. Each bubble represents a (set of) candidate(s) with the height indicating the corresponding energy level. The two lower-most states are the two distinct optimal solutions with their color emphasizing the distinct mapping of Y_0 to either Z_0 (blue) or Z_1 (yellow). An arrow between two bubbles indicates a direct connection between

Table 3: Relative sizes of energy levels

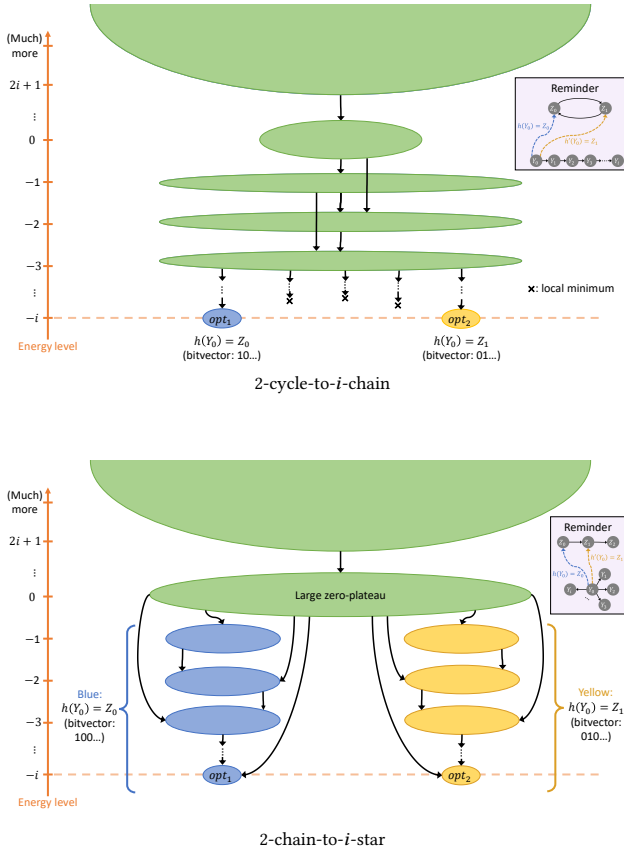
(a) 2-cycle to i -chain				
i	# bin. vars	$p_i(\text{pos})$	$p_i(\text{neg} \neg\text{pos})$	$p_i(0 \neg\text{pos})$
1	4	~ 44%	~ 22%	~ 78%
2	6	~ 58%	~ 37%	~ 63%
3	8	~ 68%	~ 49%	~ 51%
4	10	~ 76%	~ 59%	~ 41%
\vdots	\vdots	\vdots	\vdots	\vdots
∞	∞	100%	100%	0%

(b) 2-chain to i -star				
i	# bin. vars	$p_i(\text{pos})$	$p_i(\text{neg} \neg\text{pos})$	$p_i(0 \neg\text{pos})$
1	6	75%	~ 13%	~ 87%
2	9	~ 88%	~ 22%	~ 78%
3	12	~ 94%	~ 29%	~ 71%
4	15	~ 97%	~ 34%	~ 66%
\vdots	\vdots	\vdots	\vdots	\vdots
∞	∞	100%	50%	50%

them, which means that they contain neighboring states. The arrows point towards the lower energy level, but there is also a low probability that the simulated annealing algorithm jumps in the reverse direction.

For *2-cycle to i-chain*, the negative energy levels are connected in a cascading/short-stepped way, such that connected neg states are at most two energy levels away from each other. This is due to the chain structure of the tuples in q_2 . Every node of q_2 is part of at most two edges (and thus of at most two tuples), which means that changing one single bit can change at most two terms in $p_{(3)}(\bar{x})$. Therefore, reaching an optimal solution from zero level takes at least $\frac{i}{2}$ steps. Moreover, the energy landscape contains a number of local minima that are not optimal, which are indicated by crosses in the figure. They exist because independent parts of each of the two optimal solutions can contribute to a negative value within the same bitvector. Such a local but not global minimum could, for example, look like *LRLRLRLRLR*, where *L* stands for 10 (mapping a node from the chain to the left node Z_0) and *R* for 01 (mapping it to the right node Z_1). The example candidate consists of three parts (*LRLRLR*; *RLRL*; *LR*) that independently look like part of an optimal solution, and only the connections between the parts are off. In general, those locally minimal (but not globally minimal) candidates look like piece-wise optimal candidates: sub-chains of size at least 2 are mapped correctly in itself (alternating between left and right) but alternate between the two optimal solutions. There is no way to decrease the value of that state without first increasing it by “unmapping” one of the nodes. These local minima occur below the energy levels of $-\frac{i}{2}$, and their number increases with growing i , which plays a role in lowering the solution probabilities for that family.

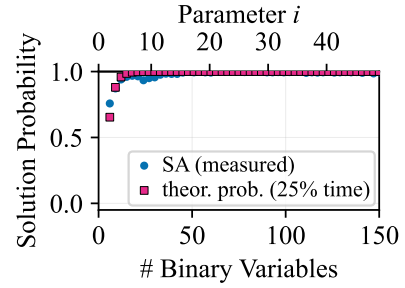
For *2-chain-to-i-star*, the neg states can be partitioned into two separate parts, half of which contain bitvectors starting with ‘100’ (central node Y_0 mapped to Z_0 , indicated in blue) and half of which


Figure 11: Energy landscapes

start with ‘010’ (central node Y_0 mapped to Z_1 , indicated in yellow). This is because the central node of the star is part of every single tuple and thus of every negative term in the polynomial. Moreover, this means that there are no local minima except for the two global minima. Every neg state can reach the next lower energy level without increasing its energy by at most two steps. If one of the nodes in $\{Y_1, \dots, Y_i\}$ has not been mapped correctly, it is either not mapped at all or incorrectly mapped. In the latter case, it can be unmapped without increasing the energy level and then correctly mapped in the next step. Regarding the first case, it can be directly mapped to reach the lower energy level. The absence of local-only minima is a key factor for the good performance observed in the experiments because the algorithm cannot get stuck.

It remains to clarify why we observe lower solution probabilities for SA in the beginning, i.e., for small values of i (cf., Figure 5b). This can be explained as follows: The neg states are highly interconnected with the zero states, since every neg state has a direct zero neighbor where the first 1 is replaced by 0 (starting with ‘000’, so the central node is unmapped). This holds specifically for the two optimal states, which also have a zero neighbor. As explained before, there is a low chance to jump out of the optimum into that higher-energy zero neighbor. For simulated annealing, we can directly compute that probability, which decreases exponentially as i grows and annealing time passes by (see Equation (8)). The counterprobability

of staying in the optimum is of the form $1 - e^{-\gamma i}$ for a constant $\gamma > 0$ (details on this are provided at the end of this section), which quickly approaches 1 for growing i . Figure 12 illustrates the probability to stay in the optimum for growing i at 25% of time and compares it to the measured solution probability of SA in the experiment that we showed in Figure 5b. Our hypothesis is that “after 25% of the time we are close to the critical point when the “escape probability” (i.e., the probability to escape from an optimal solution) is still high enough to have an impact, but afterward quickly vanishes. This is backed up by the correlation between the two scatter plots shown in Figure 12. In combination with the relatively large zero plateau for small i , jumping out of the optimum can cause the algorithm to get lost afterward, since the transition probability between states of the same energy level is always 1 (because then we have $c - c_{\text{new}} = 0$ and $e^0 = 1$, cf. Equation (8)) and thus the algorithm can move to other zero states after escaping the optimum. Putting it all together, this explains the lower solution probabilities observed for small i and their growth as i increases. For exact computations of the probabilities depicted in Figure 12, see the end of the next paragraph.


Figure 12: Measured solution probability (using SA simulator) vs. the theoretical probability for 2-chain-to-i-star to stay in optimal solution at 25% of the annealing time

Exact formulas for relative sizes and escape probabilities. The relative sizes of the different state portions are computed as follows. A state \bar{x} has a positive value if $p_{\text{fct}}(\bar{x}) > 0$, i.e., if the bit-matrix contains a row with at least two ones. For 2-cycle to i -chain, each row has length 2, so in three out of four possible 2-bit row-vectors, the row as at most one 1. The portion of pos states is given by the counterprobability of all rows having at most one 1:

$$\begin{aligned} p_i^{(\text{chain})}(\text{pos}) &= 1 - p_i^{(\text{chain})}(\neg\text{pos}) \\ &= 1 - p_i^{(\text{chain})}(\neg\text{pos}_{\text{row}})^{i+1} = 1 - \left(\frac{3}{4}\right)^{i+1} \end{aligned}$$

where $i+1$ comes from the number of rows in the bit-matrix.

Analogously, the probability for 2-chain to i -star can be computed with a row-length of 3, which leads to

$$p_i^{(\text{star})}(\text{pos}) = 1 - \left(\frac{1}{2}\right)^{i+1}$$

because in half of the eight possible 3-bit row-vectors, the row has at most one 1.

Investigating only non-positive states (which is expressed in the following by using a conditional probability: $p(\dots|\neg\text{pos})$), we can further analyze their proportions. Since each row contains at most

one 1, each row Y_ℓ can be interpreted as a mapping of the node Y_ℓ , either to nothing (zero vector) or to one of the variables Z_k from 2-cycle or 2-chain, respectively.

In the case of 2-cycle to i -chain, the state is negative if at least two consecutive nodes from the i -chain are mapped to opposite nodes from the 2-cycle. Abstractly, we can think of having an alphabet $\Sigma := \{N, L, R\}$ and the language $L_i := \Sigma^{i+1} \cap (*(LR|RL)*)$ containing all words of length $i+1$ that contain the sub-word LR or RL , which represents the portion of neg states. The size of that language can be computed (see <https://oeis.org/A193519>; accessed 2025/12/02) and is given by

$$|L_i| = \frac{1}{2} \cdot \left(2 \cdot 3^{i+1} - (1+\sqrt{2})^{i+2} - (1-\sqrt{2})^{i+2} \right).$$

The resulting fraction of all words of length $i+1$ is then given by

$$p_i^{(\text{chain})}(\text{neg}|\neg\text{pos}) = \frac{1}{2 \cdot 3^{i+1}} \cdot \left(2 \cdot 3^{i+1} - (1+\sqrt{2})^{i+2} - (1-\sqrt{2})^{i+2} \right)$$

which can also be written as $p_i^{(\text{chain})}(\text{neg}|\neg\text{pos}) =$

$$1 - \left(\frac{1+\sqrt{2}}{2} \cdot \left(\frac{1+\sqrt{2}}{3} \right)^{i+1} + \frac{1-\sqrt{2}}{2} \cdot \left(\frac{1-\sqrt{2}}{3} \right)^{i+1} \right)$$

and approaches 1 as i increases. Therefore, the opposite portion of zero states approaches 0.

In the case of 2-chain to i -star, a state has a negative value if either the central node Y_0 of the i -star is mapped to Z_0 and at least one of the other nodes is mapped to Z_1 , or if Y_0 is mapped to Z_1 and at least one of the other nodes is mapped to Z_2 . Given a correct mapping of the central node, each other node has a probability of $\frac{3}{4}$ to not follow suit. So the fraction of zero states, given that each row has at most one 1, can be computed by

$$p_i^{(\text{star})}(0|\neg\text{pos}) = \frac{1}{2} + \frac{1}{2} \cdot \left(\frac{3}{4} \right)^i = \frac{1}{2} \left(1 + \left(\frac{3}{4} \right)^i \right),$$

for which the probability of mapping the central node incorrectly is added to the probability of mapping the central node correctly, but all other nodes incorrectly. The counterpart fraction of neg states is given by the counterprobability

$$p_i^{(\text{star})}(\text{neg}|\neg\text{pos}) = \frac{1}{2} \left(1 - \left(\frac{3}{4} \right)^i \right).$$

For growing i , their ratio approaches 50/50.

This explains how we computed the numbers in Table 3. Next, we explain the computations required to understand Figure 12.

We assume that an optimal state has been reached and want to compute the probability to escape into the zero plateau when the algorithm encounters a zero neighbor. Following Algorithm 1, this means that \bar{x} is an optimal state and \bar{x}_{new} is a zero neighbor. For their energy levels, we have $c = -i$ and $c_{\text{new}} = 0$, so the probability of transition can be computed by $\text{AcceptProb}(T, i)$ with the given cooling schedule T . In the code implementation, the schedule's min and max are given by the values $\beta_{\text{start}} = \frac{1}{T_{\text{high}} k_b} := 0.5$ and $\beta_{\text{end}} = \frac{1}{T_{\text{low}} k_b} := 10$ and the algorithm follows a geometric schedule divided into 1000 steps, which means that for $\ell \in \mathbb{N}$ with $1 \leq \ell \leq 1000$, we can compute

$$\alpha = \sqrt[1000]{\frac{\beta_{\text{end}}}{\beta_{\text{start}}}} \quad \text{and} \quad \beta_\ell = \beta_{\text{start}} \cdot \alpha^\ell.$$

The accept probability for the energy difference of i at 25% of the annealing time is then given by

$$\text{AcceptProb}(T_{25\%}, i) = e^{-\beta_{25\%} \cdot i} = e^{-0.5 \cdot \sqrt[4]{20} \cdot i},$$

where $T_{25\%}$ indicates using β at 25% of the time, which is (due to using 1000 steps) given by $\beta_{25\%}$. Taking the counterprobability $1 - e^{-\beta_{25\%} \cdot i}$ we have finally arrived at the probability of staying in the optimal solution after 25% of the annealing time depending on i , which is shown in Figure 12.